Mesozoic tectonic evolution of the Daba Shan Thrust Belt in the southern Qinling orogen, central China: Constraints from surface geology and reflection seismology

Jianhua Li[1,2], Shuwen Dong[1], An Yin[3,4], Yueqiao Zhang[1], and Wei Shi[1]

[1]Institute of Geomechanics, Chinese Academy of Geological Sciences, Beijing, China, [2]Department of Earth Sciences, James Lee Science Building, University of Hong Kong, Hong Kong, [3]Department of Earth, Planetary, and Space Sciences and the Institute of Planets and Exoplanets, University of California, Los Angeles, California, USA, [4]Structural Geology Group, China University of Geosciences, Beijing, China

Abstract The Daba Shan Thrust Belt is located along the southern margin of the Qinling orogen that separates the north China block in the north from the south China block in the south. Despite decades of research, the total magnitude of shortening accommodated by continent-continent convergence across the Qinling orogen after Triassic ocean closure between north and south China remains poorly constrained. The lack of knowledge on the shortening magnitude in turn limits our ability to test a wide array of tectonic models for the development of the Qinling orogen and thus the convergence history between north and south China. In order to address this issue, we construct a balanced cross section and develop a new kinematic model for the evolution of the Daba Shan Thrust Belt. This work was accomplished by integrating (1) surface geologic mapping, (2) detailed kinematic analysis of key structures, (3) existing geochronologic and thermochronological data, and (4) a recently obtained lithospheric-scale seismic reflection profile. Restoration of the cross section indicates that the minimum shortening strain increases northward from ~10% in the foreland to >45% in the thrust belt interior. The estimated amount of upper crustal shortening across the Daba Shan Thrust Belt is >130 km, which is sufficient to allow the inferred mafic lower crust of the subducted south China lithosphere to have experienced eclogite phase transition. Thus, our work supports that the development of the Daba Shan Thrust Belt may have been driven by slab pull of the subducted mafic lower crust at the leading edge of the down-plunging south China continental lithosphere.

1. Introduction

The Paleozoic to Jurassic development of the Qinling orogen in central China has resulted from protracted oceanic subduction, ocean closure, collision/accretion of microcontinents and island terranes between the north and south China blocks, and postocean closure continent-continent convergence [e.g., *Yin and Nie*, 1993; *Meng and Zhang*, 2000; *Zhang et al.*, 2001; *Ratschbacher et al.*, 2003]. The southern margin of the orogen is marked by the arcuate Triassic-Jurassic Daba Shan Thrust Belt, which is ~300 km long and up to 120 km wide [*Zhang et al.*, 2001; *Dong et al.*, 2013]. Surface mapping, detailed structural analysis, and geochronological studies indicate that the development of the Daba Shan Thrust Belt continued over a period of >60 Ma, with significant crustal contraction occurring episodically at two discrete time intervals: (1) earlier contraction took place in the Middle-Late Triassic when the collision between north and south China occurred in response to diachronous closure of their intervening Paleo-Tethyan oceans and (2) later contraction took place in the Middle-Late Jurassic in response to the continued convergence between the north and south China Blocks [*Zhang et al.*, 2001; *Ratschbacher et al.*, 2003; *Li et al.*, 2013]. The Jurassic continued convergence between the north China and south China Blocks is puzzling, as the Paleo-Tethyan oceans to the west (i.e., the Kunlun Shan region of central Tibet) and to the east (i.e., Dabie Shan, eastern Shandong, and central Korean peninsula) were already closed by the end of the Triassic, which means that the slab pull by oceanic subduction along the same convergence margin could not have been the main driving mechanism of the continued subduction [e.g., *Yin and Nie*, 1996]. Currently, two competing mechanisms have been proposed to explain the long-lasting (>60 Ma) convergence between north China and south China: (1) it was driven by collision between south China and terranes to the south such as Qiangtang and Lhasa [*Yin and Nie*, 1996] and (2) it was induced by slab pull of eclogitized mafic lower crust of south China [*Dong et al.*, 2013].

In order to unravel the architecture of the Daba Shan Thrust Belt rimming the southern margin of the Qinling orogen, a crustal-scale seismic reflection profile was acquired. A preliminary interpretation of this seismic image was presented by *Dong et al.* [2013] who show that (1) strong reflectors in the middle and lower crust are truncated by transparent regions interpreted as plutons, (2) Neoproterozoic strata were deposited over a group of older fault-bounded Precambrian rift basins, and (3) the Daba Shan Thrust Belt is bounded by a regionally extensive, north dipping décollement that can be traced to a depth of >27 km. In general, the work of *Dong et al.* [2013] emphasizes strongly on the general structural style and tectonic development of the Daba Shan Thrust Belt. However, no efforts were made in that study to use the deep seismic profile to quantify the total amount of shortening across the Daba Shan Thrust Belt. The lack of knowledge on the shortening strain across the Daba Shan directly impacts our ability to differentiate the competing mechanisms for driving the continued continent-continent convergence across the Qinling orogen. For example, the frontal slab pull hypothesis of *Dong et al.* [2013] requires the inferred mafic lower crust of south China to have been subducted below a depth of 40–70 km where the pressure and temperature conditions favor phase change of mafic rocks (presumably in the lower crust of the northern margin of south China [see *Dong et al.*, 2013]) to the denser ecologite [e.g., *Hacker et al.*, 2011]. In contrast, the far-field stress transmission induced by collision along the southern margin of south China [e.g., *Yin and Nie*, 1996] does not require significant crustal shortening across the Daba Shan Thrust Belt.

In order to determine the magnitude of crustal shortening across the Daba Shan and to test the feasibility of the frontal slab pull model of *Dong et al.* [2013], we integrate surface mapping, kinematic analysis of key structures, synthesis of existing geochronologic and thermochronologic data, and more importantly, systematically analyze the crustal-scale seismic reflection profile of *Dong et al.* [2013]. The detailed analysis of the seismic reflection profile represents the first effort in quantifying the magnitude of deformation associated with the development of the Qinling orogen during the phase of continent-continent convergence. As described in detail below, we achieve this goal by constructing a retrodeformable balanced cross section at a lithospheric scale across the Daba Shan Thrust Belt.

2. Regional Geology

2.1. Tectonic History of the Qinling Orogen

Phanerozoic development of the Qinling orogen occurred predominately in two stages, first during the ocean closure along the Shangdan suture in the Paleozoic in the north and subsequently along the Mianlue suture in the Triassic in the south [*Meng and Zhang*, 2000; *Zhang et al.*, 2001]. The Shangdan ocean was established before 540 Ma as a branch of the Proto-Tethyan ocean [*Dong et al.*, 2011; *Pei et al.*, 2005, 2007]. It was subsequently closed as a result of the South Qinling terrane colliding with the North Qinling terrane along a north dipping subduction zone [*Ratschbacher et al.*, 2003, 2006]. This event was accompanied by multiple episodes of (ultra) high-pressure and (ultra) high-temperature metamorphism [e.g., *Bader et al.*, 2013]. Final closure of the Shangdan ocean between the North and South Qinling terranes occurred in the Early Devonian (~400 Ma) [*Meng and Zhang*, 2000; *Zhang et al.*, 2001].

The Mianlue ocean began to open during the Devonian closure of the Shangdan ocean [*Meng and Zhang*, 1999; *Dong et al.*, 1999, 2004]. This ocean was closed diachronously from west to east from the late Early Permian to the Triassic as a result of counterclockwise rotation and northward penetration of the south China Block relative to the north China block [*Zhao and Coe*, 1987; *Enkin et al.*, 1992; *Yin and Nie*, 1993; *Gilder and Courtillot*, 1997; *Hacker et al.*, 2000, 2004]. Final collision of the united north China craton, including the North and South Qinling terranes, and the south China craton occurred in the Late Triassic along the Mianlue suture that extends eastward to the Dabie Shan, Shandong, and Korean peninsula [e.g., *Yin and Nie*, 1993, 1996; *Hacker and Wang*, 1995; *Hacker et al.*, 1998, 2006; *Ratschbacher et al.*, 2003; *Zhang et al.*, 2004]. The continuous convergence between north and south China in the Jurassic was expressed by shortening and strike-slip faulting within the Qinling orogen [*Wang et al.*, 2003; *Li et al.*, 2013].

The Daba Shan Thrust Belt was developed as a foreland thrust system of the Qinling orogen [*Dong et al.*, 2013]. The thrust belt displays an arcuate shape in map view and trends generally in the northwest direction (Figure 1) [*Zhang et al.*, 2001; *Ratschbacher et al.*, 2003]. The Daba Shan Thrust Belt involves Archean to Jurassic rocks and locally Cretaceous strata (Figure 1); the involvement of Cretaceous strata indicates the longevity of the thrust belt from the Triassic to possibly Cenozoic [*Dong et al.*, 2013;
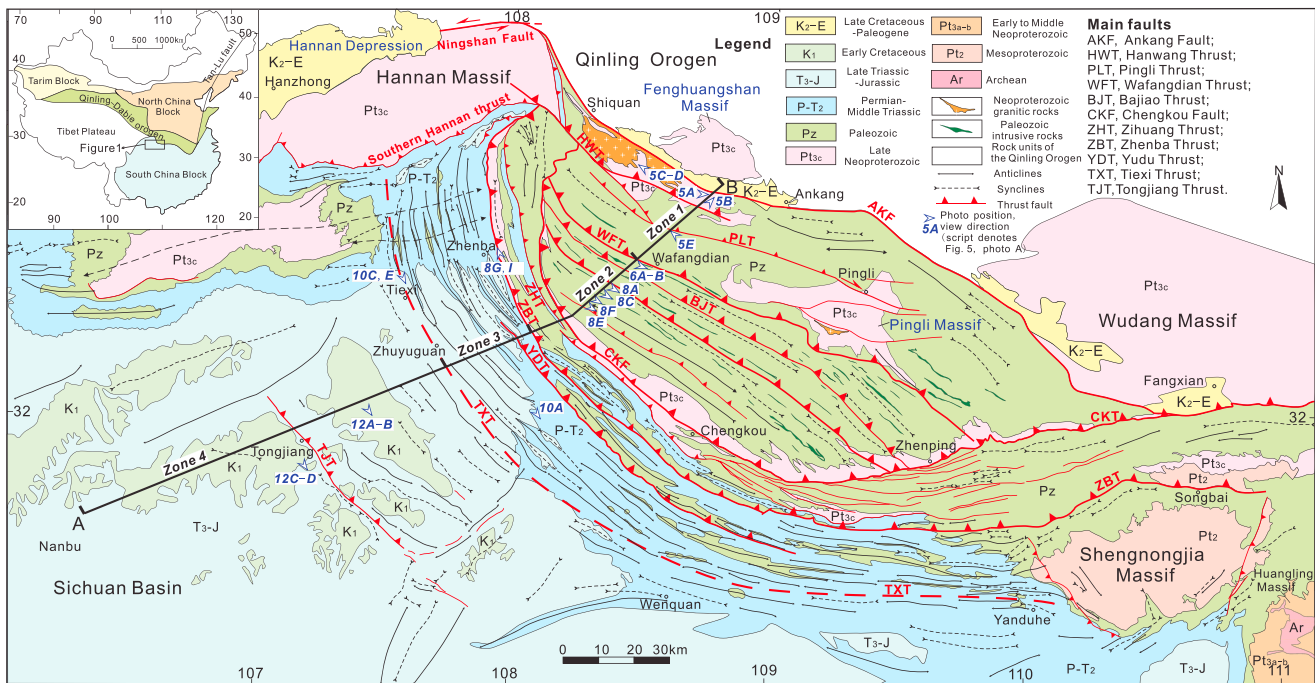
Figure 1. Simplified tectonic map of the Daba Shan-north Sichuan Basin fold-thrust belt and location of cross section for field mapping and seismic reflection profiling. Inset map shows that the Qinling orogen separates north and south China cratons. The ductile Ankang fault marks the boundary between the Qinling orogen and the Daba Shan Thrust Belt.

Enkelmann et al., 2006]. The arcuate trace of the Daba Shan Thrust Belt, though at a much smaller scale, is quite similar to the geometry of the 2000 km long Himalayan arc, as both are marked by the presence of syntaxes at their lateral terminations [e.g., *Yin*, 2006; *Dong et al.*, 2013]. Unlike the Himalayan arc [e.g., *Taylor and Yin*, 2009; *Yin*, 2010], there are no arc-perpendicular normal faults coeval with the thrust belt development present in the Daba Shan area.

2.2. Tectonic Division of the Daba Shan Thrust Belt

Three faults can be traced from one end to the other along the entire strike of the Daba Shan Thrust Belt. From north to south they are (1) the Ankang fault (AKF), (2) the Chengkou fault (CKF), and (3) the Zhenba thrust (ZBT) (Figure 1). All three faults dip to the north, with the northernmost Ankang fault marking the northern edge of the Daba Shan Thrust Belt. The current trace of the Ankang fault is a north dipping Cenozoic transtensional structure that places Cretaceous and Paleogene strata in the north over the Archean to Paleozoic strata in the south (Figure 1). The regionally extensive Chengkou and Zhenba thrusts divide the Daba Shan Thrust Belt into three thrust sheets: the thrust sheet in the footwall of the Zhenba thrust, the thrust sheet in the hanging wall of the Zhenba thrust, and the thrust sheet in the hanging wall of the Chengkou thrust. The Chengkou fault is the basal décollement of an imbricate thrust system, which is expressed in map view by termination of straight-traced thrusts at this arcuate-shaped fault (Figure 1). The arcuate versus straight fault traces suggest that the Chengkou fault has a gentler dip than the dips of its hanging wall thrusts.

These major faults, coupled with the blind Tiexi thrust (TXT), divide the Daba Shan Thrust Belt into four zones that display distinctly different structural styles from each other (Figure 1). Zone 1 consists of widely spaced (20–25 km) thrusts involving Archean to Mesoproterozoic metamorphic basement of south China; zone 2 consists of closely spaced (5–10 km) imbricate thrusts in the hanging wall of the Zhenba thrust; zone 3 is dominated by folds involving Permian to Jurassic strata; and zone 4 consists of open folds and minor thrusts involving Jurassic and Cretaceous strata (Figure 1). Given that zone 4 evolved into the foreland depression in response to thrust loading and development of the Daba Shan Thrust Belt during the Middle Jurassic to Early Cretaceous time [e.g., *Hu et al.*, 2012; *Shi et al.*, 2012], we assign it to be part of the Daba Shan Thrust Belt although the thrust structures are scarcely developed at its surface.
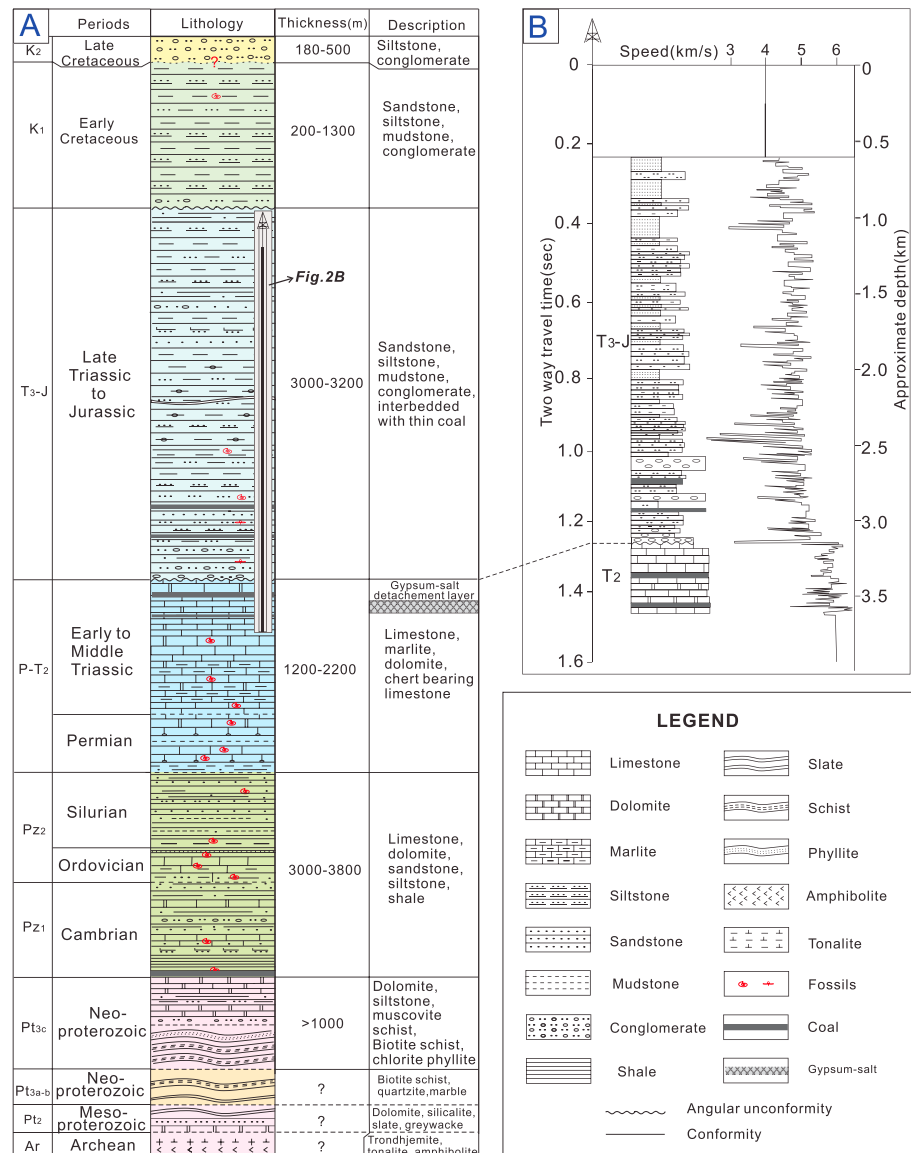
Figure 2. (a) Lithostratigraphic column of major rock units in the Daba Shan and neighboring regions. (b) Detailed stratigraphic information on the Middle Triassic to Lower Jurassic stratigraphy obtained from drill hole data (modified after *Liu et al.* [2006], see Figure 3 for location).

2.3. Lithologic Units of the Daba Shan Thrust Belt

The age of rock units involved in the thrust belt becomes progressively younger southward, from Archean to Proterozoic in the north to Cretaceous in the south (Figure 1). This relationship indicates that the basal décollement dips to the north, allowing deeper rocks to be brought up to the surface along a series of north facing ramps branching off from the detachment. In order to assist cross-section construction, we compile the age and thickness of all stratigraphic units exposed in the Daba Shan Thrust Belt based on the existing literatures and published geologic maps [*Liu et al.*, 2006; *Li et al.*, 2009, 2010; *Lu and Qu*, 1987; *Cheng et al.*, 1988; *Shanxi Bureau of Geology and Mineral Resources* (*SBGMR*), 1989; *Hubei Bureau of Geology and Mineral Resources*, 1990] (Figure 2).

The Archean unit known as the Kongling metamorphic complex is exposed in the Huangling massif at the eastern end of the Daba Shan (Figure 1). It consists of ~3.2 Ga bimodal gneisses of tonalite, trondhjemite, granodiorite (TTG), and amphibolite [*Qiu et al.*, 2000; *Liu et al.*, 2008; *Jiao et al.*, 2009; *Li et al.*, 2014].
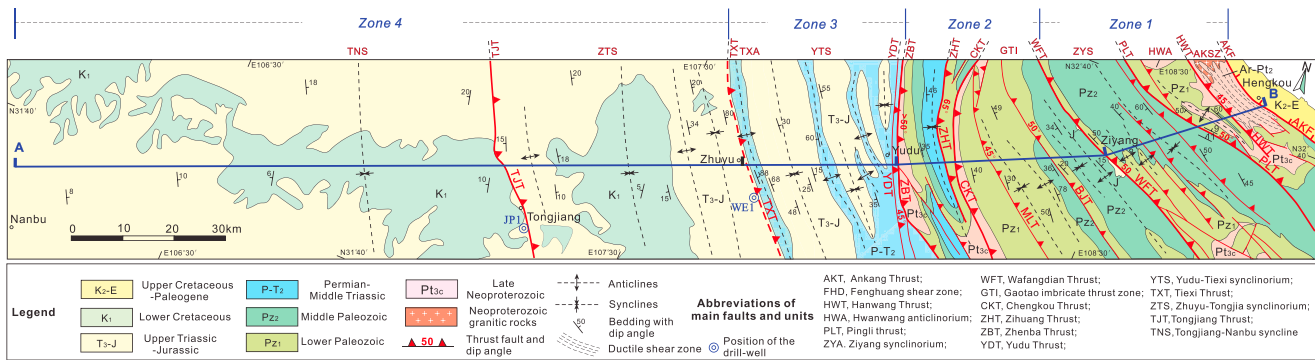
Figure 3. Simplified geologic map showing key structural data obtained from field mapping in this study. The data, integrated with seismic reflection image, are used for cross-section interpretation and reconstruction.

The Mesoproterozoic sequence (Pt$_2$), exposed in the Shengnongjia massif (Figure 1), comprises pelagic dolomite, siliciclastic rocks, and greywacke-slate assemblages and are interbedded with 1.1 Ga tuff layers (Figure 2) [*Li et al.*, 2009; *Deng et al.*, 2013]. The Neoproterozoic sequence consists of two lithostratigraphic units termed Pt$_{3a-3b}$ and Pt$_{3c}$ in this study. The former is exposed mainly in the Huangling metamorphic massif and overlies Archean TTG assemblages (Figure 1). The latter, cropping out in the Fenghuangshan and Pingli massifs and along the Chengkou thrust (CKT) in zones 1 and 2 (Figure 1), comprises >1000 m thick greenschist facies metavolcanic and metasedimentary rocks (Figure 2a) that were intruded by 790–740 Ma granitiods [*Li et al.*, 2012]. These low-grade metamorphic rocks are intensively folded and constitute the folded basement of the Daba Shan, which are in turn overlain by the Paleozoic-Triassic marine cover sequence. The Paleozoic sequence (Pz$_{1-2}$) is best exposed in the northern part of the Daba Shan Thrust Belt and consists of 3000–3800 m thick marine carbonates (Figure 2a). The lower part of the sequence (Lower Paleozoic, P$_{Z1}$) is composed of Cambrian limestone, dolomite, sandstone, siltstone, and shale [*Wang et al.*, 1989; *SBGMR*, 1989], whereas the upper part (Middle Paleozoic, P$_{Z2}$) is composed of Ordovician-Silurian fossiliferous limestone, shale, and sandstone (Figure 2a) [*Yan et al.*, 2011; *Cheng et al.*, 1988]. The above rock sequence is extensively cut by Silurian (440–420 Ma) gabbroic dykes (Figure 1) [*Luo and Duanmu*, 2001; *Zou et al.*, 2011], which originated from crustal rifting along the northern margin of south China [*He et al.*, 1999; *Zhang et al.*, 2010].

Younger Permian to Cretaceous strata exposed in zones 3 and 4 (Figure 1) can be further divided into four stratigraphic sequences (Figure 2a). The Permian to Middle Triassic sequence (P-T$_2$) is 1200–2200 m thick and composed of marine carbonate and include gypsum- and salt-bearing limestone, dolomite, and marl limestone (Figure 2a) [*Wang and Zhou*, 1988]. The salt layer therein acts as a main décollement surface that accommodates distributed layer-parallel contraction and differential deformation above and below [*Tang et al.*, 2007]. Although the Triassic sequence was deposited continuously in time [*Meng et al.*, 2005], a dramatic facies change occurred at the end of the Middle Triassic when deposition of marine carbonates was switched to deposition of terrigenous clastic strata [*Mei et al.*, 2010]. The Upper Triassic to Jurassic (T$_3$-J) terrigenous sequence is extensively distributed in the Sichuan Basin (Figure 1). The information on the lithology and thickness of this sequence comes from a deep well (WE1) drilled by the Sinopec Oil Company at the southern end of zone 3 from *Liu et al.* [2006] (Figure 2b; also see Figures 3 and 4 for its location). This well reaches a depth of ~3500 m that penetrates entirely the Upper Triassic to Jurassic terrigenous deposits and reveals that this sequence is up to 3200 m thick and comprises sandstone, conglomerate, and mudstone (Figure 2b) [*Liu et al.*, 2006]. The folded Upper Triassic to Jurassic sequence is unconformably overlain by Lower Cretaceous (K$_1$) red beds that are ~1200–1300 m thick and consist of sandstone and mudstone [*Dong et al.*, 2006] (Figure 2a). This unconformity supports the identification of an important Middle-Late Jurassic crustal shortening event in the Daba Shan Thrust Belt [*Dong et al.*, 2006]. The Upper Cretaceous sequence (K$_2$) is locally exposed in the hanging wall of the Ankang fault and consists of red sandstone and conglomerate, with a thickness of 180–500 m [*SBGMR*, 1989] (Figure 2a). The contact between the Lower and Upper Cretaceous sequences has not been observed.
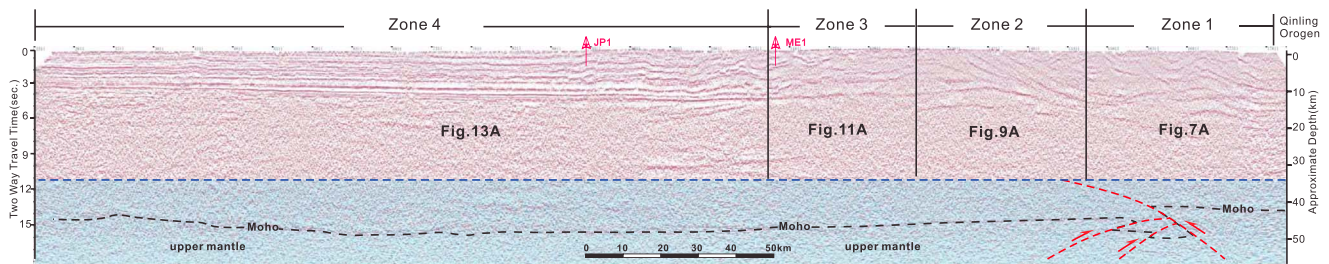
Figure 4. Uninterpreted high-resolution seismic prolife across the Daba Shan Thrust Belt. The seismic reflection data were collected by the Southern Exploration and Development Division Company of SINOPEC.

3. Data Collection and Data Analysis

Field mapping was conducted along a >310 km long traverse across the Daba Shan Thrust Belt (transection A-B in Figure 3). The mapping route follows closely the seismic reflection profile of *Dong et al.* [2013]. Attitudes of foliation, bedding, fold hinges, shear zones, and faults were measured systematically along the traverse (Figure 3). The kinematics of major shear zones and faults were determined in the field or via examination of thin sections.

The >310 km long seismic reflection profile of *Dong et al.* [2013] shown in Figure 4 was acquired in 2007 from the Southern Exploration and Development Division Company of SINOPEC. Data acquisitions and data processing were discussed in *Dong et al.* [2013]. In the display of the seismic profile used for constructing balanced cross sections, we show both the two-way traveltime sections and the approximately corresponding depths converted from assigning an average seismic velocity of 6 km/s (Figure 4). As the velocity of the seismic image varies with depth from about 4.5–5 km/s to 6.8–7.1 km/s from top to the base of the crust, this simple time-depth conversion may distort the true geometry of the imaged structures in the upper and lower crustal sections [*Li et al.*, 2006]. This in turn affects the estimates of horizontal shortening when using the line balancing method. Based on the regional knowledge of seismic velocity variation with depth [*Li et al.*, 2006], the assignment of seismic speed at 6 km/s would stretch the uppermost 5 km of the crust for about 20–30% and compressed the lowermost crust and the upper mantle for about 10–30% vertically. It is straightforward to show that this effect distorts the length of a gently inclined surface (dip angle is < 20–30°) by no more than 5% of its original length [*Gao et al.*, 2013]. Notably, the reflector sequence marking the crust-mantle transition in zones 3 and 4 is undulate and continuous, whereas in zones 1 and 2 is discontinuous and placed vertically (Figure 4). This observation implies that the Moho had been duplicated by thrust faulting, which was interpreted as resulting from Jurassic Daba Shan thrusting by *Dong et al.* [2013]. Given that the mode of Moho deformation has been discussed in *Dong et al.* [2013], this study focuses primarily on revealing and interpreting the mode of crustal deformation.

In order to construct a balanced cross section across the Daba Shan Thrust Belt, we project surface geology downward into the seismic profile. For the units that are not exposed at the surface, we use the information shown in Figure 2 to project the thickness of the units that underlie the units exposed at the surface. The positions of the stratigraphic units at depths are also controlled by drill hole data, mostly from the foreland region in the Sichuan Basin. The positions of the wells are projected onto the cross sections (Figure 4).

The geometric and kinematic plausibility of the constructed cross section was tested by step-by-step palinspastic restoration. The restoration was done by removing the effect of sequential deformation from the youngest to oldest events following the procedures of *Murphy et al.* [1997], *Kapp et al.* [2003], *Yin et al.* [2007, 2008a, 2008b], and *Webb* [2013]. The fold geometry in the cross section was constructed using the dip domain method of *Suppe* [1983] based on the bedding attitudes measured at the surface. Flexural-slip folding mechanism is assumed when restoring fold-induced deformation in sedimentary strata. Displacements on thrusts shown in the balanced cross sections are estimated by matching hanging wall and footwall cutoffs, whereas the crustal shortening is estimated using Lower Paleozoic strata as a maker horizon. Due to the effects of erosion that removed the hanging wall ramps, development of cleavage that accommodates shortening via pressure solution, and small-scale folding and thrusting that are not accounted for [e.g., *Yin et al.*, 2010], the estimated shortening presented in this study represents only minimum possible values.
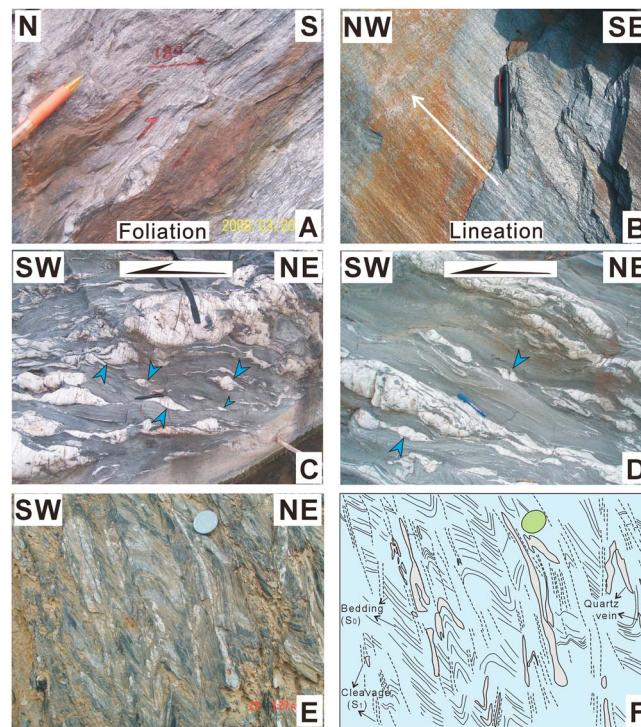
Figure 5. Field photos of rock types, common structures, and kinematic indicators in fault and shear zones observed in zone 1. Locations of the pictures and viewing directions are shown in Figure 1. (a and b) Mylonitic foliation and mineral stretching lineation in Neoproterozoic metamorphic rocks. (c and d) Sigmoidal quartz lenses and interlayered quartz vein with asymmetric tails indicating a top-to-the-SW thrust sense within the NE trending ductile Ankang shear zone. (e and f) Axial cleavage in Paleozoic slates transposed its original beddings.

4. Geologic Transect Across the Daba Shan Thrust Belt

In this section, we systematically describe the relationship between surface geology and corresponding segments of the Daba Shan seismic profile from north to south. Based on the surface geologic relationships and geometric relationships displayed in the seismic images, we discuss possible geologic interpretations of the structures at a crustal scale. The plausibility of interpretations of the cross section is tested by restorability and compatibility with the regional geologic history.

4.1. Zone 1 of the Daba Shan Thrust Belt
4.1.1. Surface Geology
The following structures are exposed in zone 1 of the Daba Shan Thrust Belt: (1) the Ankang fault (AKF) and Ankang shear zone (AKSZ), (2) the Hanwang thrust (HWT), (3) the Hanwang anticlinorium (HWA), (4) the Pingli thrust (PLT), (5) the Ziyang Synclinorium (ZYS), and (6) the Wafangdian thrust (WFT) (Figure 3).

The NE trending Ankang fault (AKF) is a south directed, moderate-dipping (~45°) structure that marks the boundary between the interior of the Qinling orogen and its Daba Shan foreland thrust belt (Figure 1). Stratigraphic relations and observed structural fabrics in the field indicate polyphase movement history of this fault zone from the Middle Triassic to the Cenozoic. Specifically, this fault zone displays top-to-the-SW and dextral ductile shear fabrics, which are interpreted to have resulted from the Middle Triassic north and south China collision and the Late Jurassic continued continental convergence, respectively [Li et al., 2013]. Subsequently, the fault surface was reactivated by normal faulting slip in the Cenozoic (Figure 3). Morphologically, the fault marks the boundary between the deeply incised Daba Shan Range in the south and the Hanzhong depression (a Cenozoic basin) in the north [e.g., Taylor and Yin, 2009] (Figure 1). Structurally below the brittle Ankang fault is the Ankang shear zone (AKSZ), which is up to 6 km wide in its central segment where we conducted our surface mapping. The shear zone is entirely restricted to Archean to Neoproterozoic basement sequences and displays intense ductile deformation and greenschist facies metamorphism (Figure 3), contrasting to brittle thrusting and fault-related folding deformation within Lower Paleozoic cover sequences in its southeastern vicinity. Shear zone deformation is characterized by NW trending, shallowly dipping mylonitic foliation (Figure 5), dip-slip stretching lineation (Figure 5b), interlayered isoclinal folds, and boudinaged quartz veins (Figures 5c and 5d). Ubiquitous kinematic indicators including asymmetrical sigmoidal veins (Figures 5c and 5d), sigmoidal porphyroclasts, and S-C fabrics indicate a top-to-the-southwest sense of shear [Li et al., 2013]. The top of the shear zone was cut and offset by the younger Cenozoic Ankang fault [Li et al., 2013].

The Hanwang thrust (HWT) is a northeast dipping, basement-involved structure that dies out northwestward into folds involving Neoproterozoic strata in map view (Figure 1). At its central segment this fault splits into two branches placing Neoproterozoic gneisses and granites over Paleozoic carbonate (Figures 1 and 3), with
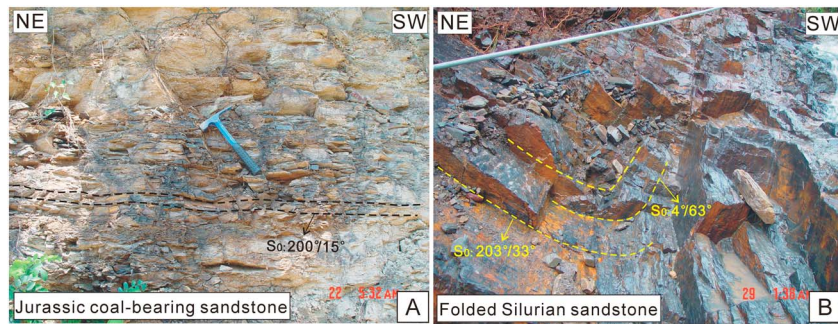
Figure 6. Field pictures that show rock units and structures below the Jurassic-Silurian unconformity in the footwall of the Wafangdian thrust. Locations of the pictures and viewing directions are shown in Figure 1. (a) Field photo of nearly flat-lying Jurassic coal-bearing sandstone beds above an unconformity. (b) Field photon of tightly folded Silurian sandstone beds below an unconformity.

the northern branch extending into Neoproterozoic folds and the southern branch linking geometrically with the Pingli thrust (PLT) (Figure 1). Directly to the southwest, the Hanwang anticlinorium (HWA) consists of two anticlines and two synclines involving Neoproterozoic to Lower Paleozoic strata (Figure 3). The anticlines bear steep to overturned southwestern limbs and moderately dipping northeastern limbs. The western anticline is interpreted as a basement-involved antiformal stack generated by successive forward migration of thrust faulting in a "piggyback" fashion by considering cross-section balancing (Figures 7a and 7b), similar to those documented in western Tibet [e.g., *Kapp et al.*, 2003].

The Pingli thrust (PLT) extends northwest that dies out laterally into folds involving Paleozoic strata (Figure 1). Along most of its trace this thrust juxtaposes structurally higher Neoproterozoic-Lower Paleozoic units over Middle Paleozoic units (Figure 3). Geometrically, this fault dips steeply (~55°) toward northeast and cuts flat-lying Paleozoic units on its two sides at a high cutoff angle of ~50°.

The Ziyang synclinorium (ZYS), located in the southwest of the Pingli thrust, consists of three synclines and two anticlines involving Middle and Lower Paleozoic strata. For the easternmost syncline, three map-scale southwest directed imbricate thrusts, branching from a folded bedding-parallel thrust fault at the base of the Middle Paleozoic (P_{Z2}), are identified from surface mapping and subsurface seismic profiling (Figures 3 and 7). Contractional structures, including cleavage, thrusts, and fault-related folds, crop out widely in this synclinorium. This style of deformation is well displayed by folding and shearing of Upper Paleozoic carbonate and greywacke as shown in Figures 5e and 5f.

The southwest directed Wafangdian thrust (WFT) carries Lower Paleozoic greywacke and shale over Lower Jurassic coal-bearing sandstone and mudstone (Figure 3), implying that the fault activity postdated the Lower Jurassic deposition. Lower Jurassic sediments in the footwall are flat lying (Figure 6a) and unconformably rest on top of the tightly folded Silurian sandstone (Figure 6b). This relationship indicates that folding of Silurian strata took place prior to the deposition of the Jurassic strata. Notably, this thrust dips at a moderate angle (~50°) to the northeast that is parallel to the overlying Lower Paleozoic strata but truncates the underlying Middle Paleozoic strata at an angle of >40° (Figure 3). This relationship requires a ramp-flat trajectory for its upward geometry when cross-section balancing is considered.

4.1.2. Subsurface Geology

The corresponding seismic reflection profile, depicting moderately to steeply dipping structures, assists us to interpret the origin of the observed surface structures. Prominent reflectors are shown in Figure 7a. In general, the upper crust is characterized by discontinuous, finely laminated, and parallel reflectors that are interpreted as representing sedimentary strata. Some reflectors appear to be folded (e.g., reflectors 1–3 in Figure 7a), whereas others appear to be truncated and/or offset by faults (e.g., reflectors 1–3 in Figure 7a). Directly below these reflectors is a region of weak reflectivity at a depth of 4–6 km that contrasts to the layered reflectors of strong reflectivity in the upper crust. At the northern end of the weak reflectivity region, a sequence of gently folded reflectors (orange triangles) can be traced (reflector A in Figure 7a). We interpret this reflector as a thrust décollement and refer it as *Decollement* 1. Although the southward extension of the décollement is unclear in the seismic profile, geometries of overlying
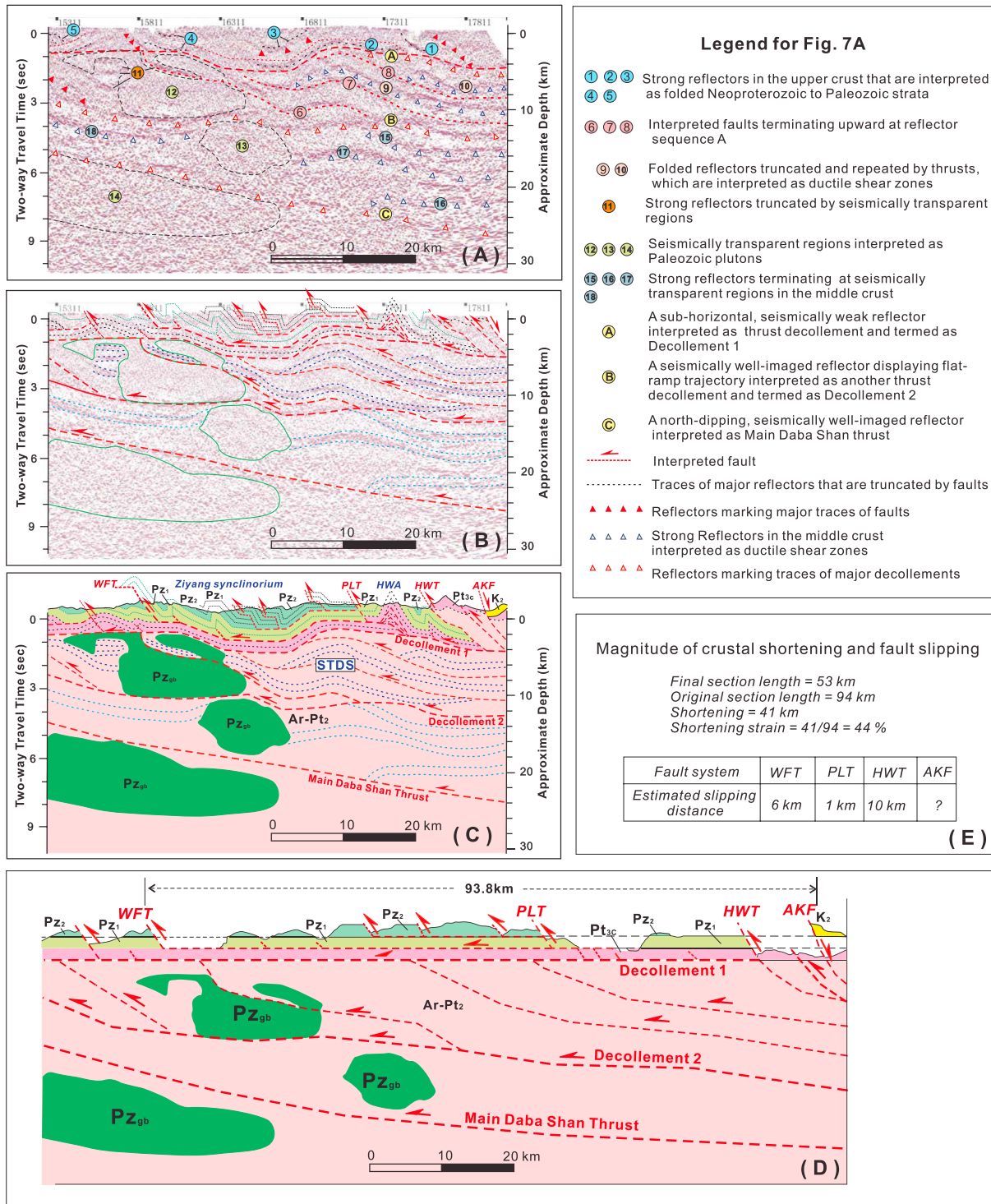
Figure 7. (a) Seismic profile showing the distribution of major reflector sequences labeled sequentially from 1 to 18 and A to C. See Figure 4 for location. The characteristics of each reflector sequence are described in the legend. (b) Interpreted section showing inferred faults and geologic contacts in the seismic profile. (c) Geological cross section constructed from the interpreted seismic profile in Figure 7b. Assignment of lithologic units is based on extrapolation of surface geology and the stratigraphic thickness information shown in Figure 2a. (d) Restored cross section of zone 1. (e) Estimated magnitude of crustal shortening and the magnitude of fault displacement.

structures require it to have been positioned within the weak reflectivity region when considering cross-section balancing (Figures 7a and 7b). The décollement also links geometrically with several minor moderate-dipping reflectors (red triangles), which we interpreted as minor branch thrusts (e.g., HWT and WFT in Figure 7c) in a southwest directed imbricate thrust system as they merge downward with Decollement 1 (Figures 7a and 7b).

One prominent reflector below Decollement 1 in the middle crust is the broadly folded low-angle reflector sequence B, which lies continuously at a depth of 9–14 km and displays flat-ramp geometry by truncating a sequence of layered reflectors in its hanging wall (i.e., reflector 6 in Figure 7a). Reflector sequence B can be traced continuously from zones 1 and 2 to below the Qinling orogen and is interpreted as another thrust décollement, herein referring as Decollement 2 responsible for accommodating midcrustal deformation. Decollements 1 and 2 probably represent the roof and floor faults of a southwest tapering duplex system (STDS) with its southern (left) end extending into zone 2. In general, the overall seismically defined structures within the duplex system exhibit strong reflectors that are broadly folded or weakly tilted before terminating at other reflectors or seismically transparent regions (i.e., reflectors 6–10 in Figure 7a). Some finely laminated reflectors, extending laterally for 30–40 km and displaying hanging wall ramp geometry (i.e., reflectors 6–8), are interpreted as minor imbricate thrusts as they climb up section from Decollement 2 and merge upward with Decollement 1. Other layered reflectors, lying ~1 km above the interpreted minor thrusts, are truncated by the thrusts (i.e., reflectors 9 and 10) or terminate abruptly at a seismically transparent region (e.g., reflector 11). We interpret these reflectors as ductile shear zones within the Archean to Proterozoic basement based on their correlation with surface geology and subsurface stratigraphic assignments complying with that shown in Figure 2a. Transparent patches (reflectors 12–14 in Figure 7a), featured by irregular boundary geometry, are observed to truncate the gently north dipping reflectors in the middle and lower crust. They are located below the Wafangdian thrust (WFT) where Paleozoic gabbroic dikes occur widely [*Luo and Duanmu*, 2001; *Zou et al.*, 2011], likely representing mafic intrusions emplaced during dike formation (Pz_{gb}) [*Dong et al.*, 2013]. Such an interpretation is further supported by high gravity and magnetic anomalies of transparent regions [*Li and Ding*, 2007; *Zhang et al.*, 2009].

Directly below Decollement 2, the density of reflectors in the middle-lower crust (15–30 km) decreases dramatically. A prominent reflector can be traced continuously in the seismic profile that lies ~5–15 km below our interpreted Decollement 2, which extends laterally for >120 km across the entire zones 1 and 2 (i.e., reflector sequence C in Figure 7a). We interpret this north dipping reflector as another thrust décollement and refer it as the Main Daba Shan Thrust following *Dong et al.* [2013]. Finely laminated reflectors between the Main Daba Shan Thrust and Decollement 2 (i.e., reflectors 15–18 in Figure 7a), extending laterally for 20–30 km, are broadly folded that display upward or downward arching geometry in the seismic reflection profile. Some reflectors appear to be truncated by décollements (reflectors 15 and 16), whereas others appear to terminate abruptly at the seismically transparent region (reflectors 17 and 18). Similar to the explanations of reflectors 9–11, these reflectors are interpreted as ductile shear zones in the middle crust that involve the Archean to Proterozoic basement of the Daba Shan (Figures 7b and 7c).

4.1.3. Cross-Section Restoration and Estimated Crustal Shortening Strain

The restored section of zone 1 is shown in Figure 7d, which allows us to estimate the total amount shortening and related shortening strain by comparing present and the original length of the deformed section. Line balancing and summation of minimum fault slip suggest a shortening amount of ~41 km across the ~94 km long cross section, which yields a shortening strain of ~44% (Figure 7e). Slipping distances along the faults are estimated by comparison of matching units across these faults. Our restoration requires the Hanwang (HWT), Pingli (PLT), and Wafangdian (WFT) thrusts to have ~10 km, ~1 km, and ~6 km of fault slip respectively to accommodate the contractional deformation within zone 1 (Figure 7e). Notably, there is no matching unit across the Ankang fault, and the Late Cretaceous unit of its hanging wall could be placed anywhere above the Neoproterozoic strata in the restored section (Figure 7d). Therefore, the exact slip on this fault is undetermined.

4.2. Zone 2 of the Daba Shan Thrust Belt

4.2.1. Surface Geology

The following major structures are exposed at the surface across zone 2 of the Daba Shan Thrust Belt: (1) the Gaotan imbricate thrust zone (GTI), (2) the southwestward convex Chengkou thrust zone (CKT), (3) the northeast dipping Zihuang thrust (ZHT), and (4) the northeast dipping Zhenba thrust (ZBT) (Figure 3).
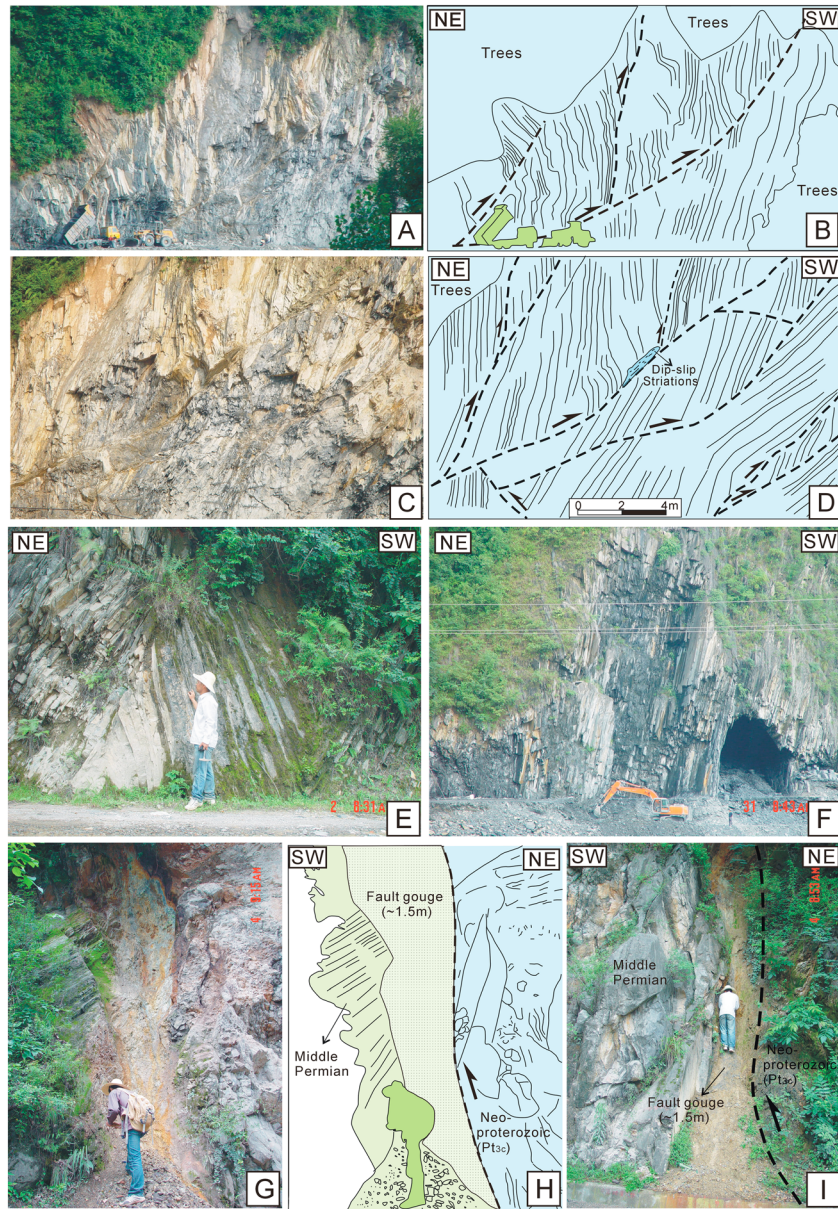
Figure 8. Field pictures showing structural styles in zone 2. Locations and viewing directions of the pictures are shown in Figure 1. (a and b) Top-to-the-SW imbricate thrusts in the Lower Paleozoic limestone. (c and d) Top-to-the-SW imbricate thrusts in the Lower Paleozoic sandstone. (e) Tight chevron folds in the Lower Paleozoic limestone. (f) The upright limb of isoclinal folds in the Lower Paleozoic limestone. (g–i) The steep-dipping Zhenba thrust places Neoproterozoic strata over Permian carbonates, beneath which ~1.5 m wide fault gouge has been generated.

The Gaotan imbricate thrust zone is bounded by the Wafangdian and Chengkou thrust zones in the north and south and consists of three southwest directed thrust sheets separated by the Bajiao and Maliu thrusts (BJT and MLT) (Figure 3). Major rock units repeated by imbricate thrusting include Neoproterozoic metavolcanic rocks and Paleozoic platform carbonates at surface (Figure 3). Outcrop-scale structures, including southwest directed imbricate thrusts (Figures 8a–8d), tight chevron folds (Figure 8e), and isoclinal folds with upright limbs (Figure 8f), are ubiquitously distributed within this imbricate system. The northwest striking Bajiao thrust dips 50° northeast that truncates broadly folded upper and lower plate beddings. This thrust juxtaposes Lower Paleozoic limestone and dolomite over Ordovician-Silurian (P_{Z2}) shale and sandstone at its central segment (Figure 3) and merges with the arcuate Chengkou thrust zone (CKT) at the two ends (Figure 1). Parallel to the Bajiao thrust (BJT), the southwest directed Maliu thrust

(MLT) dips 45° northeast that offsets moderate-dipping Lower Paleozoic layers and merges laterally at two ends with the Chengkou thrust zone (Figures 1 and 3). We note that the Wafangdian, Bajiao, and Maliu thrusts share common linking geometry with the Chengkou thrust zone in map view, probably implying that the Chengkou thrust zone is a much deeper, larger décollement, with which the three parallel thrusts might have merged downward at depth.

The Chengkou thrust zone (CKT) is the most dominant structure in the Daba Shan Thrust Belt, which has a prominent convex-to-southwest oroclinal geometry that extends >250 km along strike and bounds a zone of linear-traced thrusts to the north in its hanging wall (Figure 1). Along most of its trace this thrust juxtaposes Neoproterozoic metavolcanic and metasedimentary rocks over a Lower Paleozoic carbonate sequence (Figure 3). Given that the thrust zone is parallel to the overlying Neoproterozoic strata but truncates the underlying Lower Paleozoic strata at a high angle (Figure 3), the exposed fault is interpreted as a hanging wall flat and footwall ramp. Such an interpretation is consistent with the seismic data that show the thrust zone to be a major décollement at a depth of ~10 km (Figures 9a–9c).

Directly to its southwest, the Zihuang thrust (ZHT) merges northwestward with the Zhenba thrust (ZBT) and dies out southeastward into folds involving Paleozoic strata (Figures 1 and 3). This thrust strikes N20°W and dips 65° northeast that carries flat-lying Neoproterozoic strata over broadly folded Permian to Middle Triassic strata at surface (Figure 3).

The Zhenba thrust zone (ZBT), parallel to the Chengkou thrust zone, is another prominent structure that can be traced along strike along the entire length of the Daba Shan Thrust Belt. The fault marks the boundary between zones 2 and 3 (Figures 1 and 3). This thrust zone exhibits arcuate-shaped geometry in map view, with the north striking end linking with the Southern Hannan thrust and the east striking end extending into folds involving Paleozoic strata (Figure 1). The thrust zone juxtaposes Neoproterozoic (Pt_{3c}) and Lower Paleozoic units over Permian to Middle Triassic strata along its western and central parts, whereas in the east it places Mesoproterozoic unit (Pt_2) over Lower Paleozoic unit (Pz_1) (Figure 1). In the field this thrust zone dips steeply (>50°) toward northeast (Figures 8g–8i) and its motion has produced a ~1.5 m wide fault gouge zone (Figures 8g–8i). Similar to the interpretation of the Chengkou fault zone, a ramp-flat geometry is required to explain the hanging wall bedding-parallel and footwall high-angle truncation relationship (Figures 9a–9c). As shown in the seismic profile (Figures 9a and 9b), the dip of this thrust zone becomes shallower downward and acts as a main décollement accommodating midcrustal brittle deformation above and ductile deformation below.

4.2.2. Subsurface Geology
In general, upper crustal reflectors in zone 2 are characterized by discontinuous, finely laminated layers (e.g., reflectors 1–4 in Figures 9a and 9b) that are interpreted as representing Paleozoic to Mesozoic sedimentary strata (Figure 9c). Another layered reflector, displaying a flat-ramp geometry in cross-section view by truncating reflector sequence 4 (i.e., reflector 5 in Figures 9a and 9b), is interpreted as a back thrust; its motion produced a hanging wall fault-bend fold (Figure 9c). This southwest dipping thrust is offset by another sequence of reflectors (reflector 6 in Figures 9a and 9b) branching off from reflector sequence A, which we interpret as the Bajiao thrust (i.e., BJT in Figure 9c).

Directly below the above mentioned reflectors, Decollement 1 (reflector sequence A) can be traced as a prominent discontinuity that separates upper crustal folds and brittle faults above from interpreted Proterozoic ductile shear zones and mafic plutons below (Figures 9a and 9b). The décollement is located at ~5 km depth at the base of Neoproterozoic strata and serves as the sole thrust of an imbricate system and fault-related folds in its hanging wall (Figure 9c). The décollement links along its southernmost (left) end with another sequence of reflectors that displays a staircase trajectory in cross-section view (i.e., reflector sequence B in Figures 9a and 9b). Reflector sequence B correlates with the surface expose of the Chengkou thrust and is interpreted as representing Decollement 2 (Figure 9c). The two décollements, in conjunction with linked minor thrusts between them, constitute a southwest tapering duplex system in the upper crust (i.e., the STDS in Figure 9c). Folded reflectors within the duplex system, interpreted as ductile shear zones (i.e., reflector 8), are duplicated by a minor northeast dipping thrust (reflector 7) climbing from Decollement 2 and merging upward with Decollement 1 (Figure 9c).

Reflector C is well imaged in the seismic profile and lies ~8 km below our interpreted Decollement 2, which extends over 60 km (Figures 9a and 9b) that can be traced downward to a depth of ~19 km and correlated
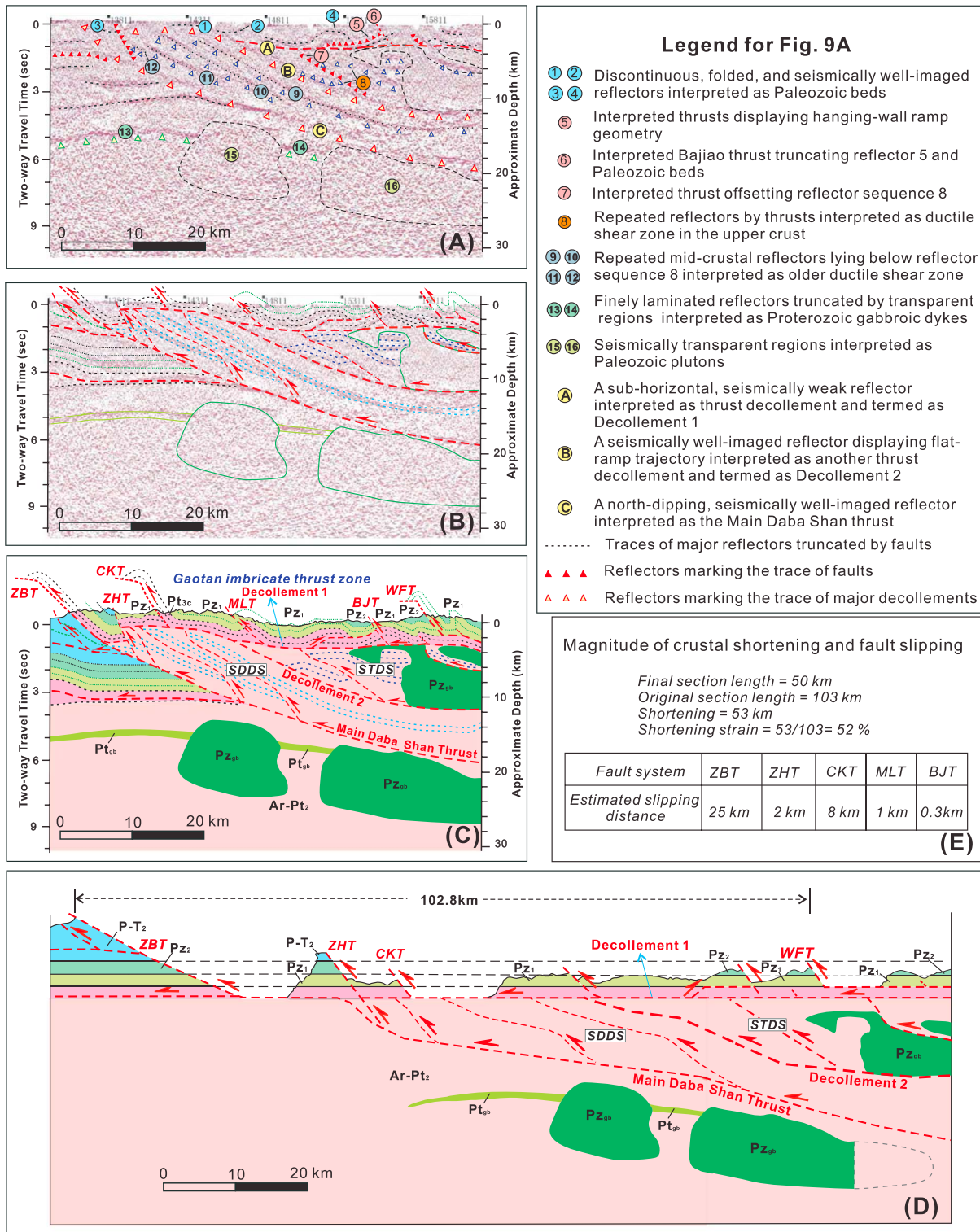
Figure 9. (a) Seismic profile showing the distribution of major reflector sequences labeled from 1 to 16 and from A to C. See Figure 4 for location. The characteristics of each reflector sequence are described in the legend. (b) Interpreted cross section showing inferred faults and geologic contacts in the seismic profile. (c) Geological cross section constructed from the interpreted seismic profile in Figure 9b. Assignment of lithologic units is based on extrapolation of surface geology and the stratigraphic thickness information shown in Figure 2a. (d) Restored cross section of zone 2. (e) Estimated magnitude of crustal shortening and fault displacement.

upward with the surface exposed of the Zhenba thrust zone (Figure 9c). We interpret this reflector also as a thrust décollement and refer it as representing the southern continuum of the Main Daba Shan Thrust (Figure 9c). Directly above this regional north dipping thrust, four parallel sequences of seismically well-imaged reflectors are present (i.e., reflectors 9–12 in Figures 9a and 9b), which terminate abruptly at margins of the seismically transparent regions associated with low seismic reflectivity. These four reflector sequences represent the southward continuum of reflector sequence 18 in Figure 7a. Although their lengths vary greatly from 3 km to 40 km, their similar reflectivity leads us to attribute them to be parts of the same ductile shear zone that was cut and repeated by imbricate thrusts (Figure 9c). If this interpretation is correct, a wider, larger, and much deeper southwest directed duplex system (i.e., the SDDS in Figure 9c) may be present at a depth of 4–19 km, with Decollement 2 and the Main Daba Shan Thrust representing the roof and floor thrusts, respectively.

Two well-imaged, discontinuous, and subhorizontal reflectors are present below the interpreted Main Daba Shan Thrust (i.e., reflectors 13 and 14 in Figure 9a). They are spaced ~1 km vertically and extend laterally for ~7 km and ~20 km before being truncated by two seismically transparent regions (i.e., reflectors 15 and 16 in Figure 9a). Following *Dong et al.* [2013], we interpret the well-imaged reflectors and transparent regions as representing Neoproterozoic mafic intrusions and Silurian (440–420 Ma) gabbroic dykes (Figure 9c).

4.2.3. Cross-Section Restoration and Estimated Crustal Shortening Strain

Each thrust sheet within zone 2 has been reconstructed to its initial position by sequential cross-section restoration (Figure 9d). The total amount of horizontal shortening calculated by line balancing of zone 2 is ~53 km across the ~103 km long cross section. This yields a total shortening strain of ~52% (Figure 9e). The minimum fault displacement is estimated at ~25 km for the Zhenba thrust zone (ZBT), ~2 km for the Zihuang thrust zone (ZHT), ~8 km for the Chengkou fault zone (CKF), ~1 km for Maliu thrust zone (MLT), and ~0.3 km for Bajiao thrust zone (BTJ), respectively (Figure 9e).

4.3. Zone 3 of the Daba Shan Thrust Belt

Zone 3 of the Daba Shan Thrust Belt is bounded by the Zhenba thrust zone (ZBT) and the Tiexi thrust zone (TXT) in the north and south (Figure 1). The zone consists mostly of folded Triassic and Jurassic strata exposed at surface (Figure 3). The assignment of geologic units in our seismic profile is based on the stratigraphic information from a deep well (WE1) penetrating through the Jurassic and Upper Triassic strata (Figure 2b). From northeast to southwest, major structures exposed in this zone include (1) the Yudu thrust zone (YDT), (2) the Yudu-Tiexi synclinorium (YTS), (3) the Tiexi anticline (TXA), and (4) the Tiexi thrust zone (TXT) (Figure 3).

4.3.1. Surface Geology

The Yudu thrust zone (YDT) places Paleozoic strata over Permian to Middle Triassic sequences along most of its trace. The fault, however, dies out laterally into folds involving Permian to Middle Triassic strata (Figure 1). The thrust strikes N30°W–N45°W and dips 45° northeast at surface (Figure 3). As shown in the seismic profile, the dip of this thrust shallows downward that eventually soles into a subhorizontal detachment within the Permian to middle Triassic strata at ~5 km depth (Figures 11a–11c).

Directly to the southwest of the Yudu thrust zone, the northwest striking Yudu-Tiexi synclinorium (YTS) consists of four synclines and three anticlines involving Permian to Jurassic strata (Figure 3). These folds exhibit various geometries at outcrop scales, which include box folds (Figures 10a and 10b), isoclinal folds, and upright to overturned folds (Figures 10c and 10d).

The northwest trending Tiexi anticline (TXA), located southwest of the Yudu-Tiexi synclinorium, is an upright isoclinal fold spanning ~5 km in wavelength and involving Middle Triassic to Jurassic strata (Figure 3). The fold has a steep to overturned southern limb. In the field a Jurassic sandstone unit is isoclinally folded, accompanied by coeval northwest striking axial cleavage (Figures 10e and 10f). The Tiexi thrust zone (TXT) is a blind structure well imaged seismically below the Tiexi anticline, which displays arcuate geometry parallel to the Chengkou thrust zone in map view and marks the boundary between the foreland fold-thrust zone (zone 3) and the foreland depression zone (zone 4) (Figure 1).

4.3.2. Subsurface Geology

In general, shallow reflectors (i.e., reflector sequences 1 and 2) traceable at 0–3 km depth are characterized by finely laminated layers that are interpreted as representing Triassic and Jurassic sedimentary strata (Figures 11a and 11b). Reflector sequence 1 along most of its trace is folded into open synclines and tight
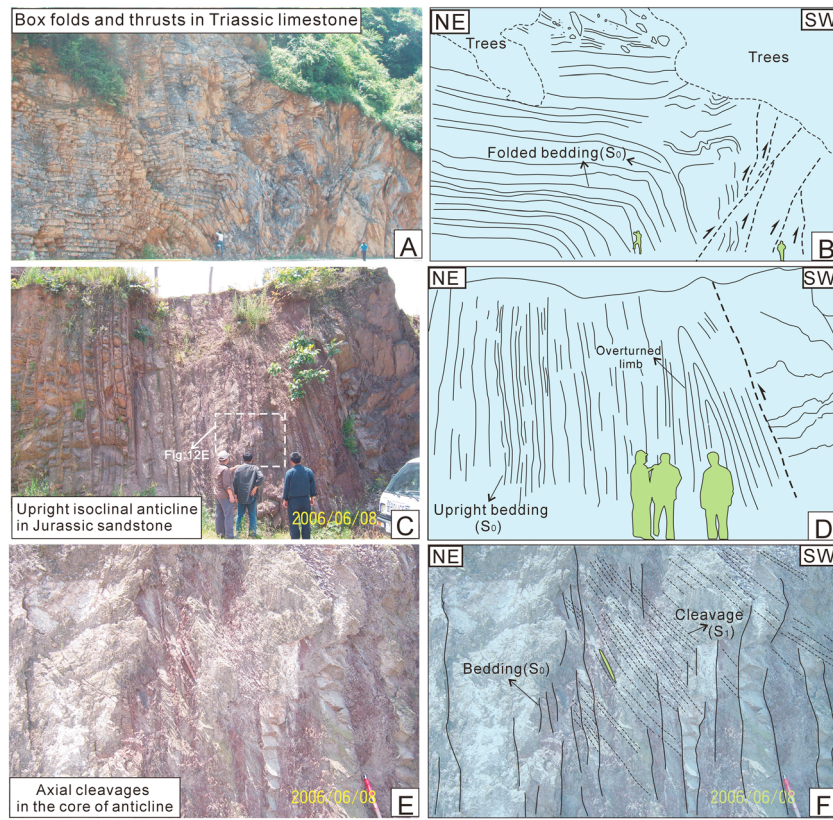
Figure 10. Field pictures showing structural styles in zone 3. Locations and viewing directions of the pictures are shown in Figure 1. (a and b) Box folds and thrusts involving the Triassic limestone. (c and d) An upright isoclinal anticline with an overturned limb in the Jurassic sandstone. (e and f) Penetrative axial cleavage in the core of an anticline.

anticlines, consistent with the folding style observed at surface. Reflector sequence 2 is flat lying and truncated by several discrete northeast and southwest directed minor thrusts branching off from an interpreted subhorizontal décollement (i.e., reflector 3) at ~3 km depth (Figure 11c). It appears that motions on the décollement and minor thrusts are responsible for the undulation of shallow reflectors that we interpreted as representing folds involving upper crustal strata. Directly below these well-imaged reflectors lies a seismically transparent region, which is spaced vertically from 3 to 6 km depth and assigned to the Permian to Middle Triassic sequence by considering stratigraphic information (Figure 2a). It is noteworthy that a salt layer exists within the Middle Triassic stratigraphic sequence that probably has acted as a main décollement surface accommodating folding and thrusting above and below [*Tang et al.*, 2007]. This requires a subhorizontal décollement to have developed in the seismically transparent region, which is marked by reflector 3 in Figure 11c. The décollement links with two back thrusts that cut up section across Upper Paleozoic strata and forms a decoupling zone separating folds and thrusts above and below (Figures 11a and 11b). The décollement is offset by an interpreted northeast directed thrust (i.e., reflector 4) that branches off from a subhorizontal back thrust (i.e., reflector 5) in the Ordovician to Silurian (P_{z2}) strata. The interpreted back thrusts (i.e., reflector sequences 4 and 5) are also observed to truncate reflector sequence 6 which we interpreted as the boundary between Middle Paleozoic (Pz_2) and Permian to middle Triassic (P-T$_2$) rock sequences.

Reflector 7 imaged in the seismic profile dips 70° NE, truncates broadly folded sedimentary strata, and terminates downward abruptly at a seismically transparent region spanning from 7 km to 11 km (marked by red triangles in Figure 11a). This reflector is assigned to the Tiexi thrust by considering its geometric association with isoclinal folds exposed at surface. This thrust might have flatten downward at the transparent region interpreted as the Neoproterozoic basement, with its northeastern (left) end merging with the Main Daba Shan Thrust at ~10 km depth. This means that the Tiexi thrust branches genetically
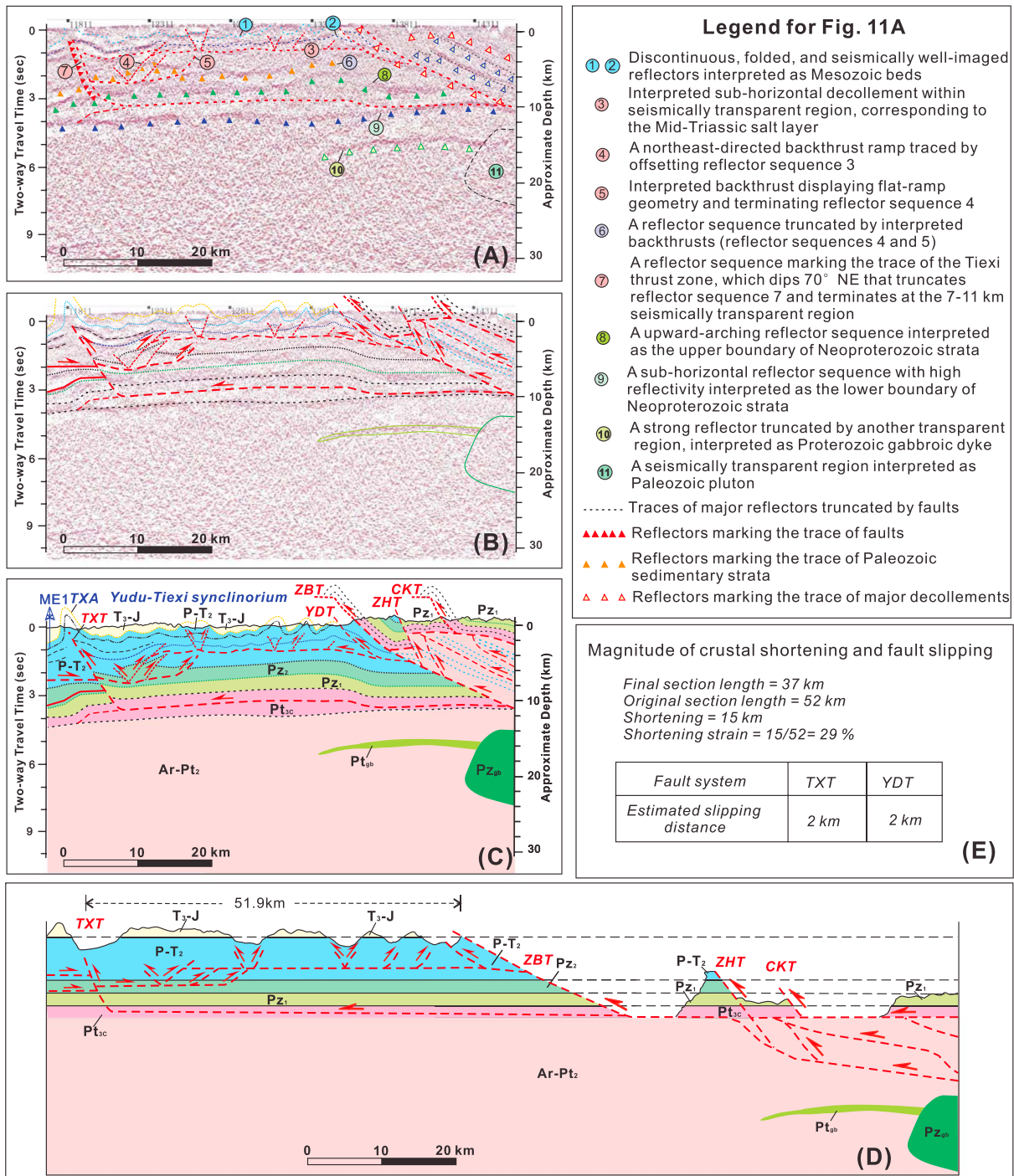
Figure 11. (a) Seismic profile showing the distribution of major reflector sequences labeled from 1 to 11. See Figure 4 for location. The characteristics of each reflector sequence are described in the legend. (b) Interpreted cross section showing inferred faults and geologic contacts in the seismic profile. (c) Geological cross section constructed from the interpreted seismic profile in Figure 11b. The assignment of lithologic units is based on surface geology and the stratigraphic thickness information shown in Figure 2a. (d) Restored cross section of zone 3. (e) Estimated magnitude of crustal shortening and fault displacement.

from the Main Daba Shan Thrust, although the two structures are parallel that appears to be geometrically unrelated to each other in map view (Figure 1). The thrust displays hanging wall ramp geometry that is responsible for upward arching geometry of reflector sequence 8 in its hanging wall (Figures 11a and 11b). Reflector sequence 8 marks the upper boundary of the Neoproterozoic strata, whereas reflector sequence 9 is traced seismically as a subhorizontal surface with high reflectivity that likely presents the
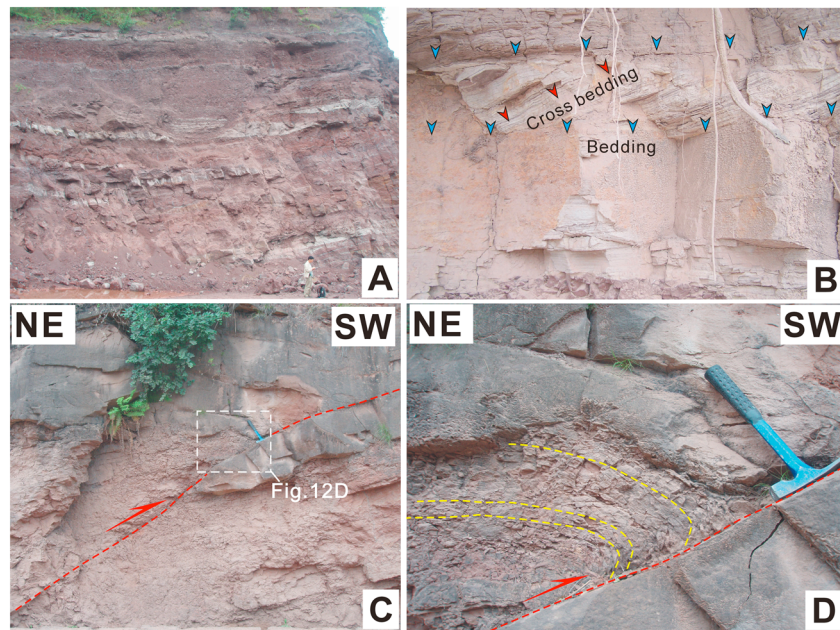
Figure 12. Field pictures showing the styles of structures in zone 4. Locations and viewing directions of the field pictures are shown in Figure 1. (a) Flat-lying to gently folded red beds in Cretaceous strata. (b) Cross-bedding sedimentary structures in Cretaceous sandstone. (c and d) Motion on a southwest directed thrust offset the Cretaceous strata and induced hanging wall fault-related folding, indicative of post-Cretaceous contractional deformation.

lower boundary of the Neoproterozoic strata (Figure 11c). Directly below this subhorizontal surface, the middle-lower crust displays sparsely distributed reflectors with low reflectivity and gives a highly transparent and empty appearance that contrasts to the seismically well-imaged upper crust (Figure 11a). The contrasting reflectivity above and below this surface is possibly induced by highly different compositions and/or mechanical behaviors between upper crustal cover rocks and middle-lower crustal crystalline basement rocks.

A flat-lying and layered reflector sequence (i.e., reflector sequence 10 in Figure 11a) lies ~6 km below reflector sequence 9. Reflector sequence 10 extends laterally for ~21 km, with the northern end being truncated by interpreted Paleozoic mafic pluton (i.e., reflector sequence 11 in Figure 11a) and the southern end terminating at the Archean-Paleoproterozoic basement. Following our previous speculation mentioned above, we interpret reflector sequence 10 as a Proterozoic gabbroic dyke intruding into the Archean-Paleoproterozoic basement rocks.

4.3.3. Cross-Section Restoration and Estimated Crustal Shortening Strain

Palinspastically restored cross section of zone 3 is shown in Figure 11d. Results of line balancing suggest that the restored section was at least 52 km long and had absorbed more than 15 km of horizontal shortening. This in turn yields a minimum shortening strain of ~29% (Figure 11e). Our restoration requires the Yudu thrust (YDT) and Tiexi thrust (TXT) to have each moved ~2 km (Figure 11e).

4.4. Zone 4 of the Daba Shan Thrust Belt

4.4.1. Surface Geology

Major structures in zone 4 include the Zhuyu-Tongjiang synclinorium (ZTS) and the Tongjiang-Nanbu syncline (TNS) separated by the Tongjiang thrust (TJT) (Figure 3). The northwest striking Zhuyu-Tongjiang synclinorium is truncated by the Tongjiang thrust (TJT) in the southwest and terminates at the Tiexi thrust (TXT) in the northeast, which exhibits broad fold geometry that spans more than 50 km in the northeast-southwest direction (Figure 3). This synclinorium consists of several open synclines and anticlines involving Upper Triassic to Lower Cretaceous strata (Figure 3). In outcrops most Early Cretaceous strata therein are expressed by flat-lying red beds without internal deformation (Figure 12a), implying that this zone has experienced no significant shortening since the Early Cretaceous. The primary sedimentary structures such as cross bedding within the red beds are well preserved (Figure 12b).
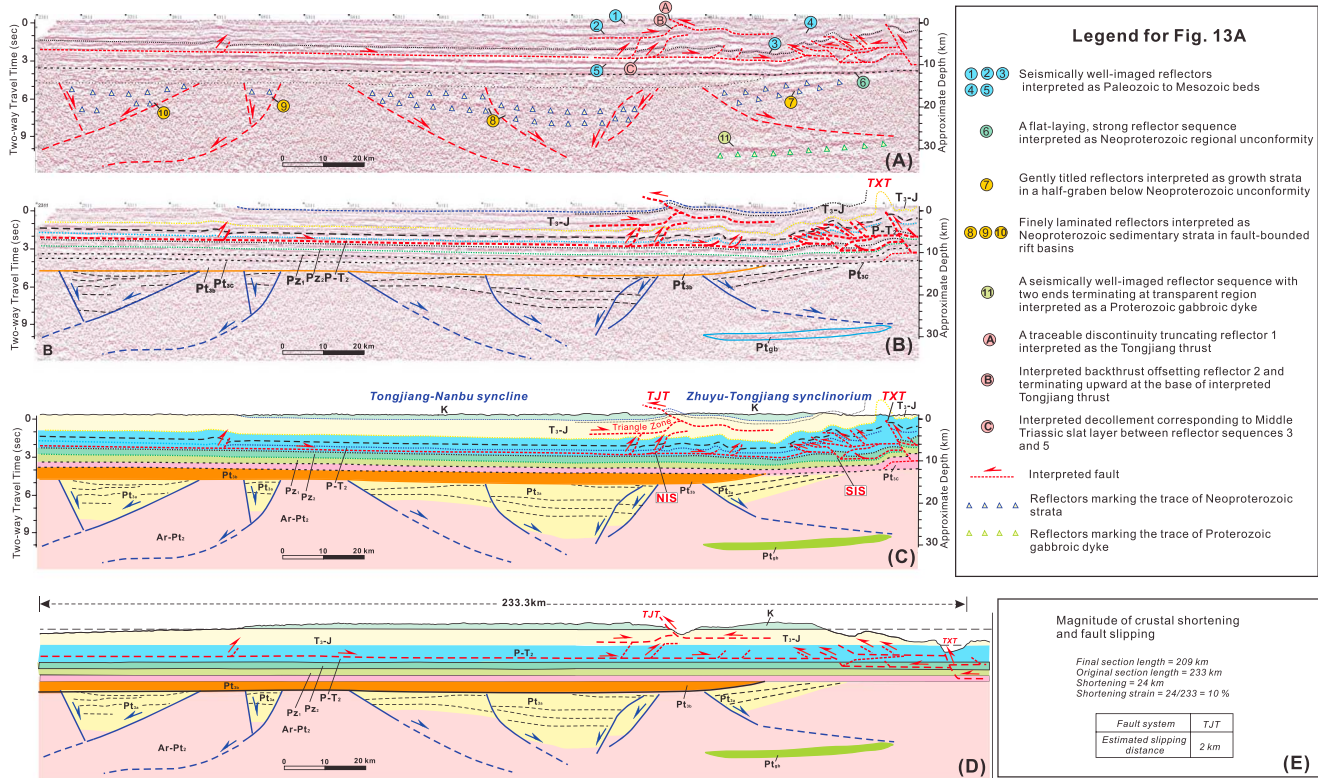
Figure 13. (a) Seismic profile showing the distributions of major reflector sequences labeled sequentially from 1 to 11 and A to C. See Figure 4 for location. The characteristics of each reflector sequence are described in the legend. (b) Interpreted cross section showing inferred faults and geologic contacts in the seismic profile. (c) Geological cross section constructed from the interpreted seismic profile in Figure 13b. The assignment of lithologic units is based on extrapolation of surface geology and the stratigraphic thickness information shown in Figure 2a. (d) Restored cross section of zone 4. (e) Estimated magnitude of crustal shortening and fault displacement.

Directly to the southwest of the synclinorium exposes the Tongjiang thrust (TJT), which strikes N50°W and dips 30° northeast parallel to its hanging wall bedding. Along most of its trace the thrust places folded Upper Jurassic strata over gently titled Lower Cretaceous strata and dies out laterally into Jurassic folds (Figure 3).

To the southwest of the Tongjiang thrust is the northwest striking Tongjiang-Nanbu syncline that involves Jurassic and Lower Cretaceous strata; it is an open fold that spans more than 100 km in the northeast-southwest direction, with both limbs dipping <20° (Figure 3). Contractional structures, featured by the development of minor thrusts and fault-related folds, are locally observed within the Lower Cretaceous red beds at outcrop scales (Figures 12c and 12d). This implies that the Daba Shan Thrust Belt underwent an episode of weak compressional deformation during or immediately after the Early Cretaceous. However, the magnitude of shortening created by the post-Cretaceous event is much less than the shortening magnitude created during the Triassic and Jurassic [e.g., *Li et al.*, 2013].

4.4.2. Subsurface Geology

Upper crustal reflector sequences are characterized by finely laminated layers that are interpreted as Paleozoic to Mesozoic strata (i.e., reflector sequences 1–5 in Figures 13a and 13b). A prominent discontinuity that can be traced at 0–3 km depth, referred as reflector sequence A, is interpreted as the Tongjiang thrust (i.e., TJT in Figure 13c). Its hanging wall reflectors are generally folded, whereas the footwall reflectors are flat lying (Figures 13a and 13b). The Tongjiang thrust offsets reflector sequence 1 and progressively flattens downward directly above reflector sequence 2. A flat-ramp thrust trajectory is implied by the staircase geometry of reflector sequence 2. In addition, the Tongjiang fault terminates the upward continuation of an underlying northeast directed back thrust (reflector B) that offsets reflector sequence 2. The two opposite-dipping thrusts constitute a northeast tapering triangle zone that accommodates shallow (0–3 km) crustal deformation in zone 4 (Figures 13a and 13b).

Directly below the triangle zone, reflector sequence 3 interpreted as Permian to Middle Triassic strata based on extrapolation of subsurface geology is truncated by four northeast directed minor back thrusts that appear to terminate abruptly at a seismically transparent region (i.e., reflector C in Figure 13a) between reflector sequences 3 and 5. We interpret the above imbricate thrusts to sole into a subhorizontal décollement, forming a northeast directed imbricate system (i.e., NIS in Figure 13c). The inferred décollement probably follows the Middle Triassic salt layer, as its position is consistent with the extrapolated depth of this marker layer when considering the regional thickness and drill hole data. To the northeast of the aforementioned imbricate thrusts, another imbricate system that is southwest directed can be traced in the seismic profile (i.e., SIS in Figure 13c). Southwest directed thrusts within this imbricate system offset reflector sequence 3, and their motions are probably also responsible for the undulation of reflector sequence 4 (Figures 13a and 13b). This imbricate system is overlain by Upper Triassic to Jurassic strata (Figure 13c), implying that the southwest directed structures were formed prior to the Late Triassic.

About 6 km below the interpreted imbricate systems (SIS and NIS) develops a continuous, subhorizontal, and high reflectivity layer termed as reflector 6, which terminates abruptly the upward continuation of south dipping reflector sequence 7 (Figure 13a). We interpret this contact relationship as a regional unconformity at a depth of ~12 km below zone 4 and assign reflector 6 to the base of Neoproterozoic strata based on extrapolation of the regional stratigraphic thickness. Below the unconformity, the dip of reflector sequence 7 decreases upward, displaying half-graben geometry; this sequence of reflectors is evidently surrounded by a pervasively transparent region (Figures 13a and 13b). Following the interpretation of *Dong et al.* [2013], we interpret the tilted reflectors to represent growth strata in a half-graben and the transparent region to represent Archean to Paleoproterozoic crystalline basement (Figure 13c). Likewise, below the central and southern parts of the unconformity, several discrete sets of finely laminated reflectors exhibit similar and weakly titled block geometry (reflector sequences 8–10 in Figure 13a). Their boundaries are less well defined in the seismic profile (Figure 13a), but they could represent normal faults similar to the interpreted structural origin for reflector sequence 7. We assign the laminated reflectors (i.e., reflector sequences 8–10 in Figure 13a) to represent Neoproterozoic (Pt_{3a}) sedimentary strata in fault-bounded rift basins (Figure 13c). Directly below the northernmost rift basin, the seismically well-imaged reflector 11 is observed to be surrounded by transparent regions (Figures 13a and 13b), which is interpreted as a Proterozoic gabbroic dike emplaced into the Archean to Paleoproterozoic crystalline basement (Figure 13c).

4.4.3. Cross-Section Restoration and Estimated Crustal Shortening Strain

Palinspastically restored cross section across zone 4 is shown in Figure 13d. The total amount of shortening calculated by line balancing of this zone is >24 km across the 233 km long cross section. This yields a total shortening strain of at least 10% (Figure 13e). Our restoration requires the Tongjiang thrust (TJT) to have moved for more than 2 km (Figure 13e).

5. Discussions

5.1. Timing of Deformation Across the Daba Shan Thrust Belt

5.1.1. Thermochronological Constraints on the Timing of Regional Thrust and Strike-Slip Faulting Within the Daba Shan Thrust Belt

In general, the thermal evolution especially accelerated cooling of thrust hanging walls provides a crucial clue to deciphering the timing of thrust faulting. A large set of samples representative of different tectonometamorphic units in the Daba Shan Thrust Belt has been analyzed by previous workers [e.g., *Ratschbacher et al.*, 2003; *Li et al.*, 2010, 2013; *Hu et al.*, 2006, 2009; *Hu*, 2011]. The closure temperatures of various thermochronometers in $^{40}Ar/^{39}Ar$ are as follows: ~550–450°C for hornblende, ~400–300°C for muscovite, ~350–250°C for biotite, and ~280–240°C for sericite [*McDougall and Harrison*, 1999]. In addition, zircon in (U-Th)/He thermochronometry has a closure temperature of 200–160°C [e.g., *Reiners et al.*, 2004] and apatite in apatite fission track thermochronometry has a closure temperature of 110–60°C [*Gleadow et al.*, 1983]. The above thermochronometers, when combined, can provide constraints on the timing of cooling, and the spatial distribution of the cooling ages in turn could be related to motion of specific structures in the Daba Shan Thrust Belt.

Hanging wall thermochronology as a proxy for the timing of thrusting has been widely used [e.g., *Yin et al.*, 1994; *Harrison et al.*, 2000]. Here we adopt the same approach to assess the thrust timing of the Chengkou fault in the
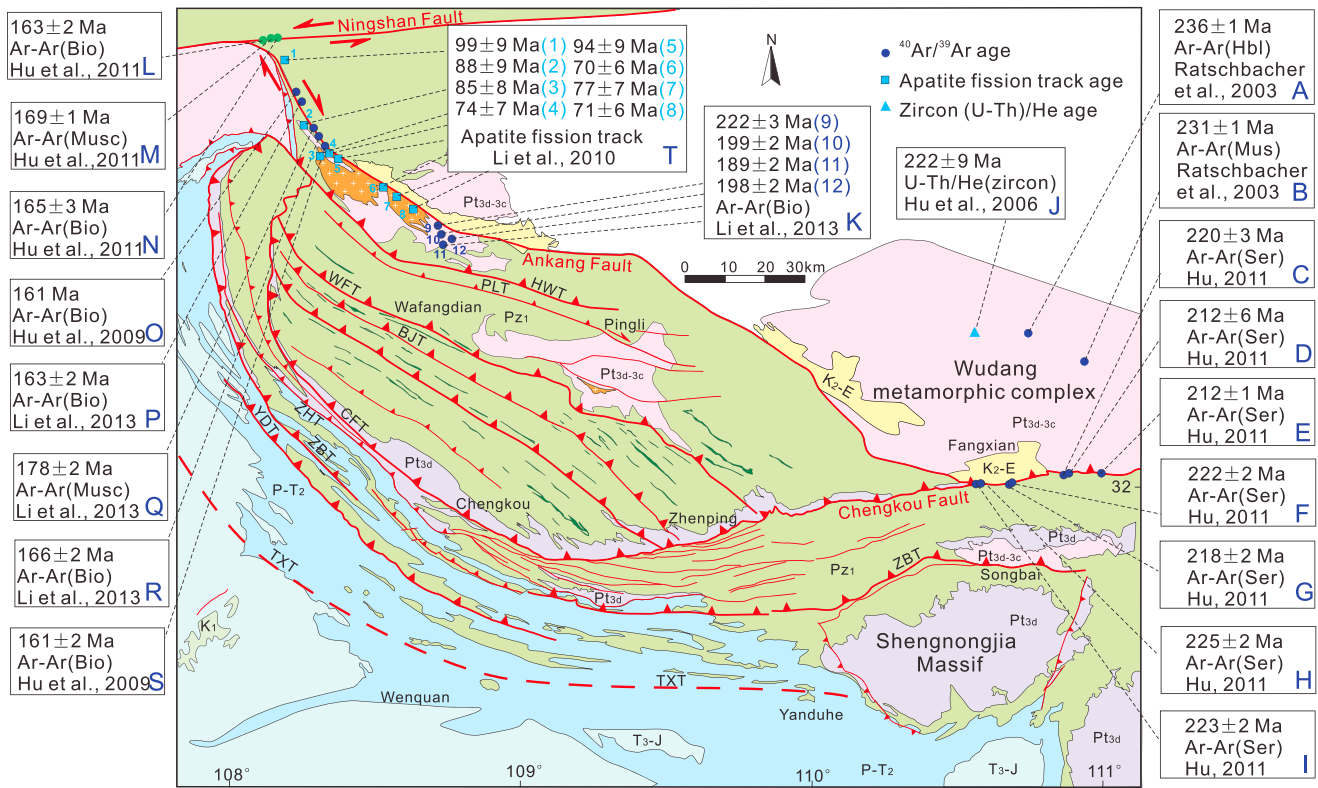
Figure 14. Simplified geological map of the Daba Shan showing available thermochronological ages that are used to constrain the timing of contractional deformation in this study. Musc, Bio, and Ser stand for muscovite, biotite, and sericite, respectively. Symbols and captions in the map are the same as in Figure 1.

Daba Shan Thrust Belt. A total of nine ^{40}Ar/^{39}Ar and zircon (U-Th)/He ages are available from the Wudang metamorphic complex in the hanging wall of the Chengkou thrust: the blueschist and metagabbro samples therein yield ^{40}Ar/^{39}Ar ages on muscovite of 231 ± 1 Ma and on hornblende of 236 ± 1 Ma, respectively [*Ratschbacher et al.*, 2003] (Figures 14a and 14b); six schist samples in the vicinity of the fault zone yield ^{40}Ar/^{39}Ar ages of 225–212 Ma for sericite [*Hu*, 2011] (Figures 14c–14i); one blueschist sample yields a zircon U-Th/He age of 222 ± 9 Ma [*Hu et al.*, 2006] (Figure 14j). Integrating with these thermochronological data, we reconstruct the thermal evolution and delineate a monotonic cooling history for hanging wall rocks of the Chengkou thrust during the Triassic (Figure 15a). Remarkably, this cooling path reveals relatively rapid cooling between circa 235 and 225 Ma, followed by slower cooling between circa 225 and 210 Ma (Figure 15a). The rapid cooling is recorded by 10 Ma difference in the hornblende and sericite ^{40}Ar/^{39}Ar ages, which requires a cooling rate of ~20°C/Ma during passage through their respective closure temperatures. This in turn corresponds to ~0.8 km/Ma denudation when the average geothermal gradient of 25°C/km is assumed. As rapid cooling of hanging wall rocks in thrust systems is commonly interpreted to be the results of thrusting-induced uplift and erosion [e.g., *Yin et al.*, 1994; *Clark et al.*, 2010], the onset of rapid cooling at circa 235 Ma may be ascribed to mark the initial motion on the Chengkou fault; the duration of rapid cooling constrains its motion between 235 and 225 Ma.

Across the hanging wall of the Hanwang thrust, four mica schist samples yield ^{40}Ar/^{39}Ar biotite ages of 222 ± 3 Ma, 199 ± 2 Ma, 198 ± 2 Ma, and 189 ± 2 Ma, respectively [*Li et al.*, 2013] (Figure 14k). The ^{40}Ar/^{39}Ar cooling ages vary as a function of the sample-site distances from the fault trace [*Li et al.*, 2013], which is expressed by a progressive increase in the cooling ages from the thrust fault to the northeast over a short distance of less than <2 km (Figure 14). This yields a very low slipping rate of <0.06 km/Ma when the slip time and distance are calculated, implying that the Hanwang thrust was nearly not active or slipped slowly during this time interval.

In addition to the age constraints from thermochronology on the thrust faults, thermochronological studies were also conducted along the right-slip Ankang ductile shear zone that lies in the hanging wall of the brittle
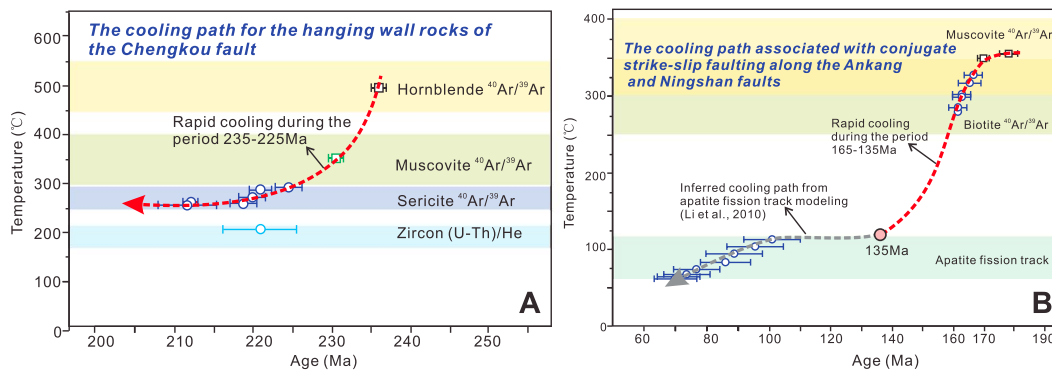
Figure 15. Reconstructed thermal evolution of major fault systems based on published thermochronological data. (a) Cooling path for the hanging wall rocks of the Chengkou fault indicates rapid cooling at ~235–225 Ma possibly related to thrusting. (b) Cooling path associated with strike-slip faulting along the Ankang and Ningshan faults. Rapid cooling at ~169–135 Ma is interpreted as resulting from transpression.

Ankang fault (Figure 14). Thermochronological data are also available across the left-slip Ningshan shear zone (Figure 14). Three metamorphic rock samples from the Ningshan shear zone yield $^{40}Ar/^{39}Ar$ ages on muscovite of 169 Ma and on biotite of 165–163 Ma [*Hu et al.*, 2011] (Figures 14l–14n); five mylonitic rock samples from the Ankang fault zone yield $^{40}Ar/^{39}Ar$ muscovite age of 178 Ma and biotite ages in the range of 166–161 Ma [*Li et al.*, 2013; *Hu et al.*, 2009] (Figures 14o–14s). These thermochronological data indicate a rapid cooling event beginning at circa 169 Ma and continuing through circa 161 Ma (Figure 15b). The ~3–8 Ma difference in the muscovite and biotite $^{40}Ar/^{39}Ar$ ages requires a cooling rate of ~33–13°C/Ma during passage through their argon closure temperatures. Moreover, apatite from eight mylonitic rock samples yield fission track ages of 99–70 Ma (Figure 14t), and their modeling results further suggest that rapid cooling did not cease till the occurrence of a 135–100 Ma slow cooling event; the latter was possibly due to a transition in tectonic regime from compression/transpression to extension [*Li et al.*, 2010]. We interpret the rapid cooling to have resulted from vertical motion due to transpression-induced exhumation of crustal slices along the restraining bends along the Ankang and Ningshan shear zones. Therefore, the duration of rapid cooling constrains the timing of strike-slip faulting on the two shear zones to be circa 169–135 Ma.

5.1.2. Geochronological and Stratigraphic Evidences From the Qinling-Dabie Orogen and the Sichuan Basin

The aforementioned thermochronological data suggest that contractional deformation within the Daba Shan Thrust Belt occurred episodically at circa 235–225 Ma and circa 165–135 Ma, respectively. Given that contractional deformation within the Daba Shan Thrust Belt must be viewed in a broad context of the tectonomagmatic evolution of the Qinling orogen and the sedimentary evolution of the Sichuan Basin [e.g., *Deng*, 1996; *Li et al.*, 2013; *Hu*, 2011], we thus review below various lines of evidence from the Qinling-Dabie orogen and the Sichuan Basin to further support our time estimates of pulsed contractional deformation across this orogenic system.

The first phase of contractional deformation within the Daba thrust belt may have been induced by the north and south China collision along the Mianlue suture in the Qinling-Dabie orogen [*Li et al.*, 2013]. The timing of this collisional event has been estimated in the Middle-Late Triassic based on (1) the U-Pb zircon ages (~245–220 Ma) of syncollisional granites (e.g., the 224 Ma Caoping granitoids of *Gong et al.* [2009], 218 Ma Wulong granite of *Jiang et al.* [2010], 214 Ma Zhashui rapakivi granite of *Hu et al.* [2004], 220–214 Ma Xinyuan and Miba monzogranites of *Sun et al.* [2000], and 245–238 Ma Xiahe and Yiliguan granitoids of *Jin et al.* [2005]) and (2) the (U)HP eclogite facies and amphibolite facies metamorphic ages (~244–220 Ma) of the Dabie-Sulu orogen [*Hacker and Wang*, 1995; *Hacker et al.*, 1998, 2000, 2006]. Our inferred early phase of contraction in the Qinling-Dabie orogen is also consistent with a regional stratigraphic relationship across the Wafangdian thrust sheet, where folded Silurian strata are overlain by the Lower Jurassic strata, implying that the folding should have occurred prior to the Early Jurassic, most probably in the Middle-Late Triassic.

The timing of our inferred second phase of contractional deformation may be constrained by the stratigraphic relationships exposed in the sedimentary evolution of the Sichuan Basin. As demonstrated by isopach maps of Mesozoic strata therein, the locus of depositional centers shifted northeastward in the
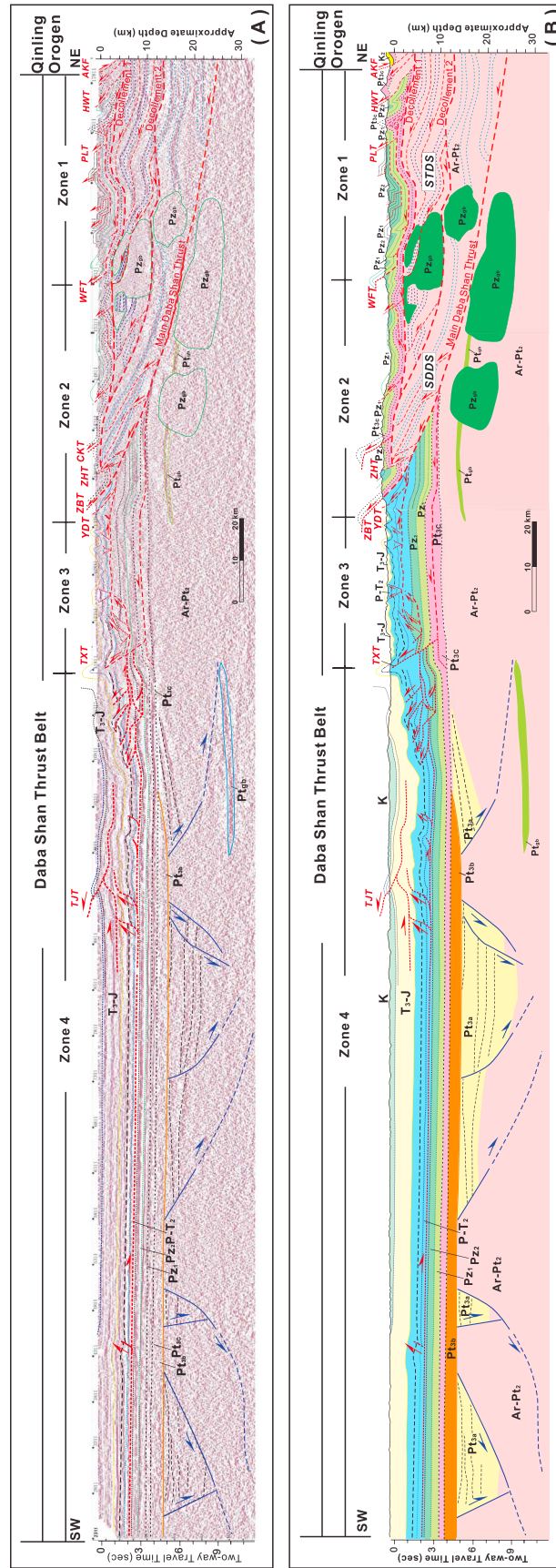
Figure 16. (a) Interpreted seismic profile showing the crustal architecture of the Daba Shan Thrust Belt. (b) Geological cross section constructed from the interpreted seismic profile in Figure 16a.
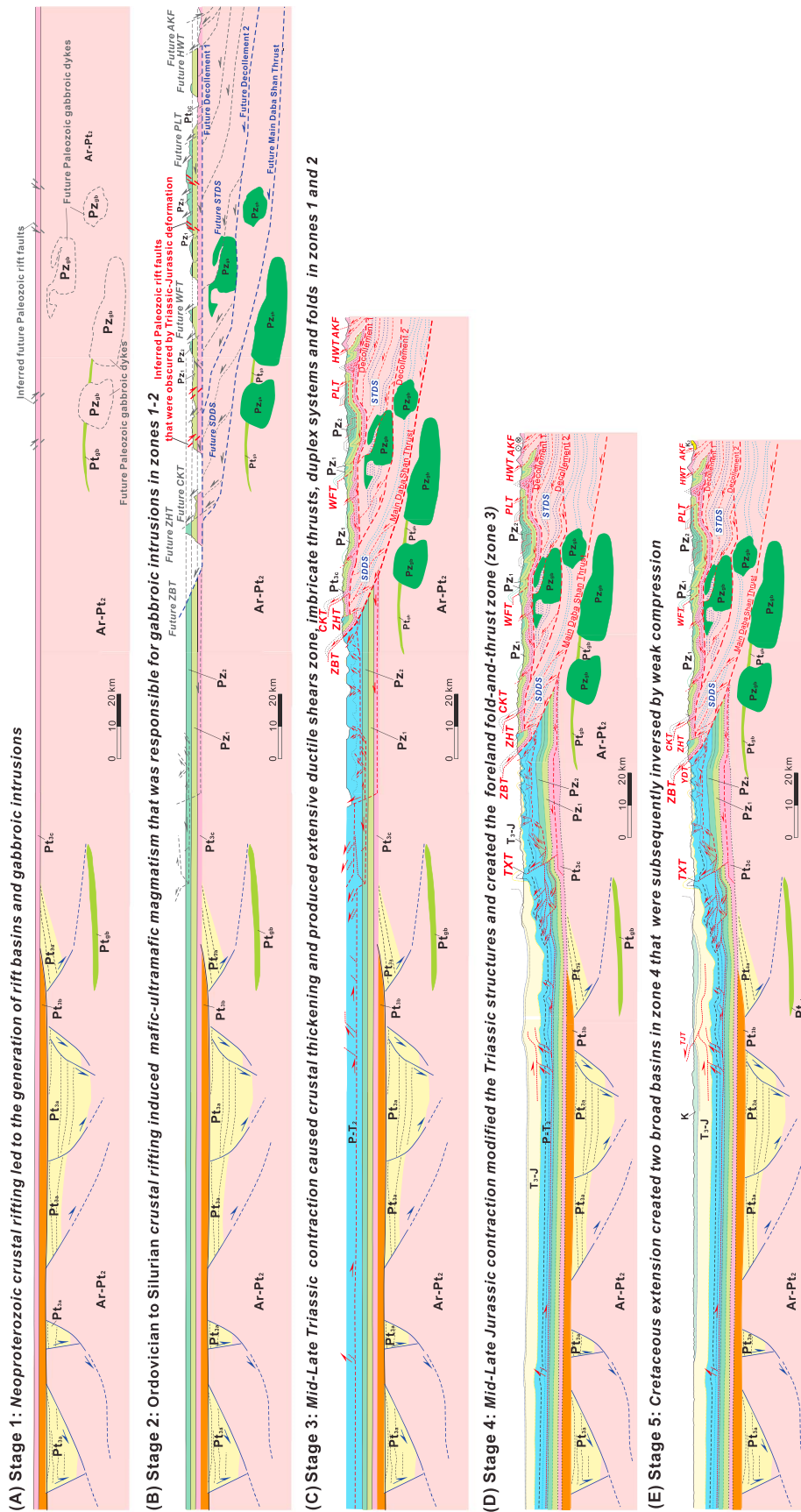
Figure 17. Kinematic reconstruction of the deformed section across the Daba Shan Thrust Belt showing the five-phase evolution during the Neoproterozoic to Cretaceous period. (a) Stage 1: A highly simplified Neoproterozoic stratigraphic framework of the Daba Shan Thrust Belt shows that the Neoproterozoic crustal rifting led to the generation of rift basins and gabbroic intrusions. (b) Stage 2: The Ordovician-Silurian crustal rifting induced extensive mafic to ultramafic magmatism that generated the 440–420 Ma gabbroic intrusions in zones 1 and 2. Future Main Daba Shan Thrust and Decollements 1 and 2 are rooted in the upper and middle crust, cutting the crystalline basement of the Daba Shan Thrust Belt. (c) Stage 3: Intense Middle-Late Triassic contraction involving the crystalline basement caused crustal thickening and modifications of the pre-Triassic rifting-related crustal architecture. Motions on the Main Daba Shan Thrust and Decollements 1 and 2 produced two vertically southwest directed duplex systems (SDDS and STDS) at a depth of 5–19 km and imbricate thrusts, fault-related folds at a near-surface depth of 0–5 km. (d) Stage 4: Middle-Late Jurassic contraction modified the Triassic structures in zones 1 and 2, and induced fault-related folding of the Triassic-Jurassic strata and coeval detachment faulting along the Middle Triassic salt layer across zone 3, eventually creating the thin-skinned fold-and-thrust zone (zone 3) in the Daba Shan foreland. (e) Stage 5: Cretaceous extension led to crustal subsidence that produced two Cretaceous basins in zone 4, and subsequently, the basins underwent weak post-Cretaceous contraction. Notably, the post-Cretaceous shortening magnitude was much less than the shortening magnitude created during the Triassic and Jurassic.

Middle-Late Jurassic [*Meng et al.*, 2005; *Richardson et al.*, 2008], which may be a result of thrust loading from the Daba Shan. In addition, the subsidence curve of the basin reveals that the subsidence rate of the Sichuan Basin increased sharply and reached its maximum (~0.2 mm/a) in the Middle-Late Jurassic [*Deng*, 1996]. The upper age bound of the second-phase contractional deformation is constrained by the contact relationship of the tightly folded Middle Jurassic strata unconformably overlain by the flat-lying Lower Cretaceous sediments [e.g., *Dong et al.*, 2006; *Shi et al.*, 2007].

5.2. Balanced Cross Section of the Daba Shan Thrust Belt

Previous work by *Dong et al.* [2013] made a preliminary interpretation on the seismic profile across the Daba Shan Thrust Belt. That work made the following first-order observations: (1) offsets of the Moho by thrusts, (2) tilted reflectors below a Neoproterozoic unconformity, (3) seismically transparent regions in the middle and lower crust that are interpreted as representing Paleozoic mafic intrusions, and (4) a regional north dipping décollement interpreted as the Main Daba Shan thrust. Our detailed results from combining surface mapping and seismic profiling allow us to construct an improved and much more detailed geologic cross section across the Daba Shan, leading to the following new insights (Figure 16). First, the Daba Shan Thrust Belt comprises thick- and thin- skinned structures separated by the Zhenba thrust (ZBT). The former involved structures that root into the crystalline basement rocks, whereas the latter are restricted entirely to the Phanerozoic sedimentary cover sequences above a subhorizontal detachment (Figures 16a and 16b). Second, contractional deformation across the Daba Shan Thrust Belt was accommodated by multiple décollement thrusting along several gently dipping stratigraphic horizons. The magnitude of the shortening strain decreases southwestward across the thrust belt (Figures 16a and 16b). Third, the shallow (<5 km) crust below zones 1 and 2 of the Daba Shan Thrust Belt is characterized by discontinuous, finely laminated seismic reflectors that correlate with exposed Proterozoic and Paleozoic strata (Figure 16a). These strata, characterized by tight folds and the presence of ductile shear zones at surface, are offset and structurally duplicated by several southwest directed imbricate thrust systems that branch off from Decollement 1 at ~5 km depth (Figure 16b). Fourth, two prominent middle-lower crustal structures across zones 1 and 2 imaged in our seismic profile, termed as Decollement 2 and the Main Daba Shan Thrust in this study (Figure 16a), correlate with the surface expose of the Chengkou and Zhenba thrust zones, respectively. These two southwest directed décollements, in conjunction with Decollement 1 and minor thrust splays, constitute two vertically stacked duplex thrust systems (i.e., the SDDS and STDS) at a depth of 5–19 km. The development of the interpreted duplex systems led to crustal thickening and formation of basement ductile shear zones (Figure 16b). Fifth, shallow (<5 km) reflectors within zone 3 are characterized by finely laminated, undulating layers (Figure 16a), which are correlative with folded Mesozoic strata observed at surface. The surface folds can be related to thrust motion across seismically imaged thrust ramps that branch off from a seismically well-imaged, subhorizontal décollement at ~4 km depth (Figure 16b). Finally, shallow crustal reflectors within zone 4 are dominantly flat lying and/or gently warped (Figure 16a), coinciding well with broadly folded Mesozoic strata exposed at surface. Directly below these open folds are out-of-sequence imbricate thrusts and in-sequence imbricate back thrusts, which are interpreted to have developed along a subhorizontal décollement along a Middle Triassic salt layer at a depth of ~8 km (Figure 16b).

5.3. Kinematic Evolution of the Daba Shan Thrust Belt

The geologic cross section presented in Figure 16b provides a basis for constructing a plausible model for the evolution of the Daba Shan Thrust Belt. Figure 17 presents a schematic five-stage tectonic history of this belt during the period from Proterozoic to Mesozoic. The first two stages, spanning from Neoproterozoic to Silurian, involved two episodes of crustal rifting that were responsible for formation of Neoproterozoic basins and emplacement of Ordovician-Silurian mafic-ultramafic magmatic bodies in the Daba Shan Thrust Belt (Figures 17a and 17b). As Neoproterozoic rift basin development and Ordovician-Silurian occurrence of mafic intrusions were discussed in detail in *Dong et al.* [2013], our tectonic reconstruction herein mainly focuses on how the Daba Shan Thrust Belt evolved in response to continental collision and convergence between north and south China in the Mesozoic.

During the Middle-Late Triassic, the Daba Shan Thrust Belt experienced intense northeast-southwest shortening, which significantly modified the pre-Triassic rifting-related structural architecture of the northern margin of south China. This event led to crustal thickening accommodated by the development

of ductile shear zones, imbricate thrusts, duplex systems, isoclinal folds, and cleavages in zones 1 and 2. Specifically, motion on major décollements produced two vertically stacked southwest directed duplex systems (i.e., the SDDS and STDS in Figure 17c) at depths of 5–19 km. Directly above the duplex systems, motion along the Decollement 1 led to southwestward propagation of contractional deformation, which is expressed by the formation of southwest directed imbricate thrusts, synclinorium, anticlinorium, and fault-related folds at 0–5 km depth (Figure 17c). Growth and development of these contractional structures are well constrained to have occurred in the Middle-Late Triassic, based on the aforementioned Jurassic stratigraphic unconformity and the 235–225 Ma rapid cooling event across zones 1 and 2. These representative contractional structures, including duplex systems, imbricate thrusts, and folds, defined the Triassic crustal architectures of zones 1 and 2. Structural development of zones 1 and 2 implies that the Daba Shan Thrust Belt evolved into the foreland fold-and-thrust zone of the Qinling orogen during the Middle-Late Triassic [*Li et al.*, 2007, 2013]. Genetically, the Middle-Late Triassic contractional deformation across the Daba Shan Thrust Belt could be ascribed to the southwestward thrust propagation of the Qinling orogen, in response to the diachronous closure of the Paleo-Tethyan Ocean and continental collision between north and south China [e.g., *Lin et al.*, 1985; *Zhao and Coe*, 1987; *Yin and Nie*, 1993; *Huang and Opdyke*, 1991; *Enkin et al.*, 1992; *Yang et al.*, 1992].

After the Middle-Late Triassic crustal contraction event, the Daba Shan Thrust Belt experienced a tectonically stable period in the Early Jurassic, with no terrane collision/accretion and crustal shortening events occurring across this belt during this time interval. This tectonic stability was further supported by coeval sedimentation in the Sichuan Basin, where the thickness of the Lower Jurassic strata was uniform throughout the basin, indicating a similar postorogenic setting characterized by tectonic quiescence during the Early Jurassic [*Meng et al.*, 2005].

Sedimentary and structural evidence suggests that tectonic activity resumed in the Middle-Late Jurassic, and the Daba Shan Thrust Belt underwent intraplate deformation and metamorphism due to the continued continental convergence between north and south China as revealed by paleomagnetic results [*Enkin et al.*, 1992; *Yang et al.*, 1992; *Nie and Rowley*, 1994; *Yokoyama et al.*, 2001]. The Middle-Late Jurassic continental convergence exerted a new force and caused extensive northeast-southwest shortening throughout the Daba Shan Thrust Belt. Specifically, to the north of the Chengkou fault, the tectonic stress produced by this event was unidirectional (NE-SW compression) that generated NW trending folds, brittle thrusts, and ductile shear zones [*Li et al.*, 2013]. These contractional structures overprint the early formed Triassic structures, as expressed by the structural juxtaposition along the Wafangdian thrust; i.e., the Lower Paleozoic rocks in the hanging wall were juxtaposed against the Lower Jurassic rocks and underlying Triassic folds involving Silurian strata in the footwall [see *Shi et al.*, 2012, Figure 12]. As the Cretaceous contraction was much tinier, zones 1 and 2 mostly illustrated consequences of structural superposing of the Middle-Late Triassic and the Middle-Late Jurassic shortening events. To the south of the Chengkou fault, the compressive stress associated with the Middle-Late Jurassic shortening event emanated radially from the Chengkou fault [*Zhang et al.*, 2010], which induced continuous, fault-related folding of the Triassic-Jurassic strata and coeval detachment faulting along the Middle Triassic salt layer across zone 3 (Figure 17d). Because the youngest rocks involved in folding and thrusting across zone 3 were the Middle Jurassic strata [*Li et al.*, 2013] and they were in turn unconformably overlain by the Lower Cretaceous rock sequence [e.g., *Dong et al.*, 2006], we inferred that the thin-skinned Daba Shan foreland orocline (zone 3) might have been created in the Middle-Late Jurassic, coevally with the development of the thrusts, folds, and fold-and-thrust structures, and in response to the strike-perpendicular, compressive stress.

As revealed by aforementioned thermochronological data (Figure 14b), the synorogenic shortening within the Daba Shan Thrust Belt might have lasted from the Middle Jurassic (~165 Ma) to the earliest Cretaceous (~135 Ma), which was eventually terminated by a subsequent postorogenic extensional event, possibly in response to gravitational instability of previously thickened crust. In map view this extension led to significant crustal subsidence that produced two broad Cretaceous basins accumulating >1000 m thick red terrestrial sediments in the foreland depression zone (Figure 17e). At the outcrop scale, this extensional event is expressed by the occurrence of NNE striking brittle normal faults that cut the Cretaceous strata and caused meter-scale offsets. Inversion of fault slip data indicates that the normal faults formed by NW-SE to W-E extension [*Shi et al.*, 2012]. Early Cretaceous extensional deformation was
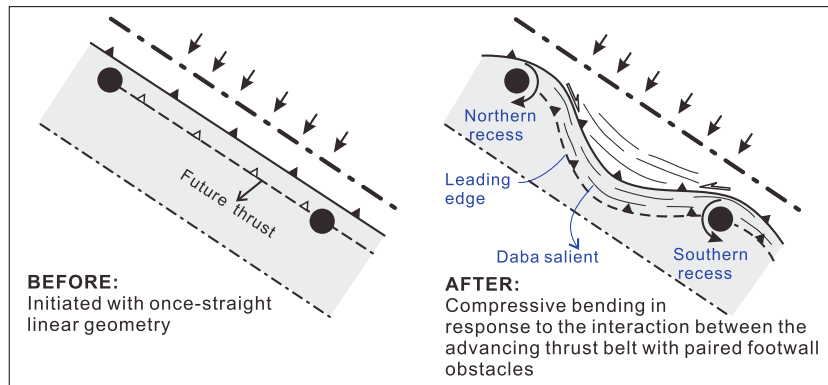
Figure 18. Structural model of obstacle-controlled orocline formation.

not only restricted to the Daba Shan Thrust Belt and seems to be widespread across the Qinling-Dabie orogen [e.g., *Ratschbacher et al.*, 2003]. This extension accommodated postorogenic crustal stretching through ductile flow, brittle-ductile, and brittle faulting events that dominated structural architecture of Hong'an-Dabie area [*Ratschbacher et al.*, 2000] and also caused extensive magmatic and metamorphic overprints that were responsible for Cretaceous unroofing in the exhumation of the Qinling-Dabie orogen [*Hacker et al.*, 1998; *Ratschbacher et al.*, 2000]. Subsequent contractional deformation postdating the Cretaceous led to basin inversion and the development of broad folds in Cretaceous strata [e.g., *Zhang et al.*, 2011] (Figure 17e). After this post-Cretaceous shortening event, the Daba Shan Thrust Belt seems to have experienced no crustal shortening during the Cenozoic, as Upper
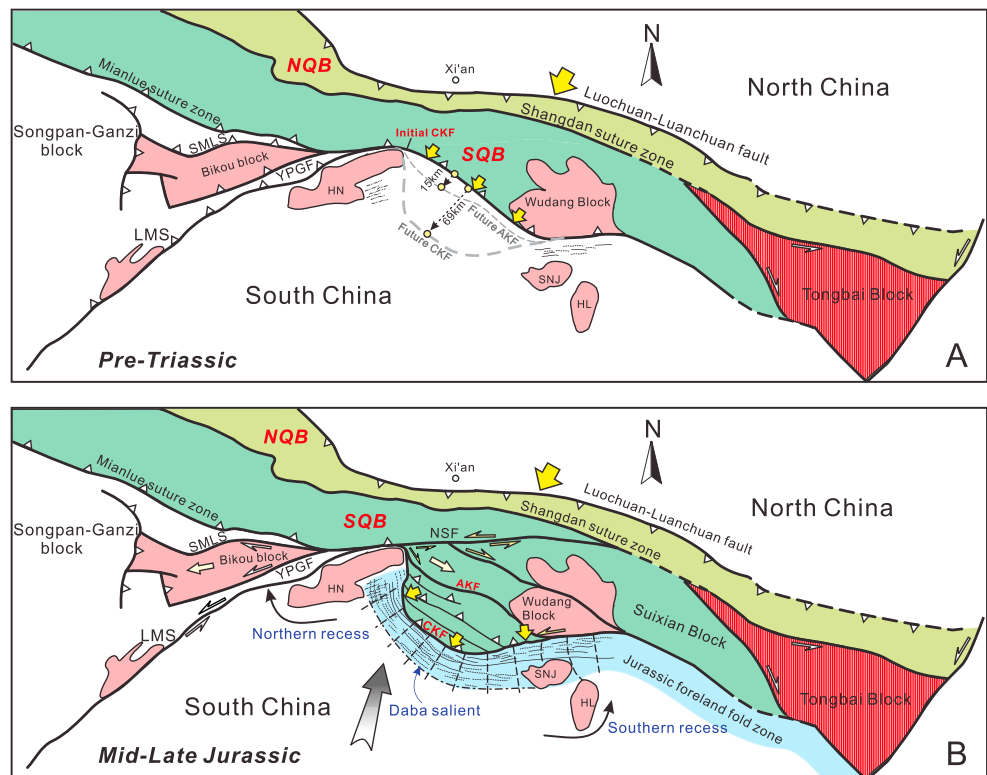

Figure 19. Schematic geological maps showing (a) palinspastically restored Daba Shan Thrust Belt and (b) its present-day geometry after Triassic-Jurassic oroclinal bending. Abbreviations: SQB = South Qinling Belt; NQB = North Qinling Belt; AKF = Ankang fault; CKF = Chengkou fault; LMS = Longmenshan fault; SMLS = South Mianlue fault; YPGF = Yangpingguan fault; HN = Hannan massif; SNJ = Shennongjia massif; and HL = Huangling massif.

Cretaceous strata therein are flat lying without internal deformation. Despite of this, the >1000 m relative elevation between the Daba Shan and Sichuan Basin, correlating closely with Cenozoic accelerated exhumation and uplifting, possibly reflects a response to eastward and lateral growth of the Tibetan Plateau in the Cenozoic and in particular to the reactivation of the Ankang fault zone [*Enkelmann et al.*, 2006; *Shen et al.*, 2007].

5.4. Tectonic Implications of Shortening Strain Across the Daba Shan Thrust Belt

Existing studies unanimously support the Mesozoic crustal contraction across the Daba Shan Thrust Belt to have been correlated with the Triassic collision and Jurassic continued convergence between north and south China [*Wang et al.*, 2003; *Li et al.*, 2007, 2013]. The slab pull model of *Dong et al.* [2013] assumes that the eclogitization of the south China lower crust together with the subducting mantle lithosphere provided negative buoyancy to drive the continued convergence between north and south China. However, this model requires that the upper crustal shortening strain must be sufficient to allow the lower crust of south China to subduct to the critical depth (~40 km) [e.g., *Spear*, 1995] where mafic rocks can be eclogitized. Palinspastic reconstruction of the cross section across the Daba Shan Thrust Belt yields a minimum horizontal shortening of ~133 km and a shortening strain of ~ 28% (estimated from Figures 7e, 9e, 11e, and 13e), which requires the same amount of lower crustal subduction of the south China block beneath the Qinling orogen and north China. Such a magnitude of shortening is sufficient to allow the mafic lower crust of the subducted south China lithosphere to have experienced eclogite facies metamorphism. Therefore, our work supports that the slab's negative buoyancy forced by lower crustal eclogitization at the trailing end of the plate might have driven the postcollisional continental convergence between north and south China.

Apart from slab pull, some researchers consider that the basal drag (or basal shear traction) could also be a major force driving plate motion and convergence [e.g., *Forsyth and Uyeda*, 1975; *Conrad and Lithgow-Bertelloni*, 2002], especially in explaining the continued Tethyan convergence and lithospheric Hagen-Poiseuille flow in the Himalayas and Tibet [e.g., *Alvarez*, 2010; *Yin and Taylor*, 2011; *McCaffrey and Nabalek*, 1998]. This model argues the lateral motion of the plates to have been caused by the mantle's exertion of a drag force on the overriding lithosphere. Such a process requires strong coupling and high viscosity between the crust and the mantle lithosphere [e.g., *Chen and Schmidt*, 2010; *Doglioni et al.*, 2007]. As the Moho below the Daba Shan Thrust Belt is offset by thrusts (Figure 4), we interpret this observation as indicating that the crust and mantle are strongly coupled because of their vertically coherent deformation. Thus, if basal shear existed, it should have played an additional role in assisting the continental subduction of south China.

5.5. Origin of the Daba Shan Foreland Orocline

Despite decades of work, how the Daba Shan foreland orocline formed and evolved remain highly disputed. The origin of the foreland orocline has been attributed either (1) to the southward thrusting of the Qinling orogen together with the pinning of basement culminations [*Zhang et al.*, 2001], (2) to the reactivation of preexisting arc-shaped boundary [*Zhang et al.*, 2010], (3) to the dextral slipping along the Mianlue suture resulting from the northward indentation of the Hannan massif [*He et al.*, 1997], or (4) to the sinistral slipping along the Mianlue suture in response to the clockwise rotation of the Shennongjia massif [*Wang et al.*, 2003]. In this study, the reconstruction of original architecture of the orocline through cross-section balancing provides additional constraints to test the above models. As discussed below, our result supports a model of progressive bending in response to the interaction between the advancing thrust belt against footwall obstacles (Figure 18).

The Daba Shan foreland orocline is bounded to the north by the Chengkou fault, and its spatial extension is characteristically parallel to the structural trend of the Chengkou fault (Figure 1), testifying to close spatial and possibly genetic associations between the two structures. This observation implies that the formation of the Daba Shan orocline can be readily ascribed to tectonic load imposed by coeval southwestward thrusting along this border fault, during and in response to southwestward thrust propagation of the Qinling orogen [*Zhang et al.*, 2001]. As revealed by cross-section restoration across zones 1 and 2 (Figures 7 and 9), contractional structures to the north of the Chengkou fault totally absorbed ~69 km of shortening during the Triassic and Jurassic. Such a shortening magnitude would require restoring the preorocline geometry of the

Chengkou fault to a NW striking linear structure located ~15 km northeast of the present-day Ankang fault (Figure 19a). Bending or buckling of this once straight structure is inferred to have developed coevally with regional southwestward thrust propagation during pulsed Triassic and Jurassic crustal shortening events, and in response to the interaction between the advancing Chengkou thrust with paired footwall obstacles, e.g., the Hannan (HN) and Shengnongjia-Huangling (SNJ-HL) basement massifs (Figure 19b). The resulting thrust load energy provided a radial, strike-perpendicular compressive stress that eventually created the SW convex foreland orocline, with the northern and southern recesses forming against obstacles and the Daba salient forming between obstacles (Figure 19b).

It is worth noting that the paired obstacles interfered with the thrust sheet, restraining its movement and giving rise to divergent transports around the obstacles, as expressed by passive rotation of obstacles around their individual vertical axis [*Wang et al.*, 2003] and accompanied transpressional deformation in the recesses (Figure 19b), similar to the structural deformation pattern observed in the Uinta Recess of central Utah, North America [e.g., *Marshak*, 2004]. Therefore, the proposed model of thrust propagation interacting with paired obstacles not only provides insights into the Daba Shan orocline formation but also explains the widespread occurrence of Middle-Late Jurassic thrusts and strike-slip structures in the northern and southern recesses [e.g., *Wang et al.*, 2003; *Li et al.*, 2013]. These transpressional structures significantly accommodated coeval lateral extrusions of major blocks (Figure 19b), including the southeastward extrusion of the South Qinling Block [*Li et al.*, 2013], the eastward extrusion of the Tongbai-Dabie Shan Belt [*Wang et al.*, 2003], and the westward extrusion of the Bikou Block [*Li et al.*, 2007].

6. Conclusions

Major geologic observations and inferences derived from surface structural mapping and deep seismic reflection profiling across the Daba Shan Thrust Belt are summarized below.

1. The Daba Shan Thrust Belt can be divided into four zones characterized by distinctly different structural patterns and deformation styles from north to south: (a) zone 1 comprises a ductile shear zone and fault-related folds involving Neoproterozoic-Paleozoic cover rocks at surface and two duplex thrust systems involving the Archean to Paleoproterozoic basement rocks at ~5–25 km depth; (b) zone 2 comprises brittle imbricate thrusts and fault-related folds involving Neoproterozoic to Paleozoic strata at surface, which shares the same duplex thrust systems with zone 1 at ~4–19 km depth; (c) zone 3 is a broad synclinorium involving Permian to Jurassic strata at surface, associated with motions along minor thrust ramps branching off from a seismically well-imaged, subhorizontal décollement at ~4 km depth; and (d) zone 4 consists of a synclinorium and a syncline involving Jurassic to Cretaceous strata at surface and several discrete fault-bounded rift basins below Neoproterozoic unconformity at ~12–25 km depth. In general, contractional deformation across these zones displays a southwestward weakening trend, changing progressively from intense ductile shearing, imbricate thrusting and tight to isoclinal folding in zones 1 and 2, to continuously broad and open folding in zones 3 and 4.
2. Structural observations, stratigraphic relationships, and thermochronological data lead us to propose that the Daba Shan Thrust Belt underwent a three-stage Mesozoic tectonic evolution after Neoproterozoic and Ordovician-Silurian rifting events: (a) Middle-Late Triassic collision between north and south China caused significant crustal shortening and produced numerous NW trending duplex systems, imbricate thrusts, and folds that constituted the Triassic crustal architecture of zones 1–2; (b) Middle-Late Jurassic intracontinental thrusting and folding that modified pre-Jurassic structures in zones 1 and 2 and created the arcuate zone 3; and (c) Cretaceous postorogenic extension and weak compression that dominated the formation and development of zone 4.
3. Palinspastic reconstruction of the cross section across the Daba Shan Thrust Belt yields a minimum horizontal shortening of ~133 km and a shortening strain of ~28%, which is sufficient to allow the mafic lower crust of the subducted south China lithosphere to have experienced eclogite phase transition. Our work supports that the slab pull produced by the eclogitization of the dominantly mafic crust at the leading edge of the subducting south China continental lithosphere may have facilitated the continued Jurassic continental convergence.
4. The Daba Shan foreland orocline was created by the interaction of an advancing thrust belt against two strong basement massifs located at the two ends of the thrust belt.

References

Alvarez, W. (2010), Protracted continental collisions argue for continental plates driven by basal traction, *Earth Planet. Sci. Lett.*, *2010*, 434–442.

Bader, T., L. Franz, L. Ratschbacher, C. de Capitani, A. A. G. Webb, Z. Yang, J. A. Pfander, M. Hofmann, and U. Linnemann (2013), The Heart of China revisited: II Early Paleozoic (ultra)high-pressure and (ultra)high-temperature metamorphic Qinling orogenic collage, *Tectonics*, *32*, 922–947, doi:10.1002/tect.20056.

Chen, J., and D. A. Schmidt (2010), Evaluating basal tractions as a mechanism of crustal rotation in the eastern syntaxis of the Tibetan Plateau, Abstract T43B-2181 presented at 2010 Fall Meeting, AGU, San Francisco, Calif.

Cheng, H. J., M. Z. Wang, X. R. Chen, A. D. Xu, and S. E. Chen (1988), A study of Ordovician system in the MTS, Dabashan [in Chinese with English abstract], *J. Xi'an Coll. Geol.*, *10*(1), 1–13.

Clark, M. K., K. A. Farley, D. W. Zheng, Z. C. Wang, and A. R. Duvall (2010), Early Cenozoic faulting of the northern Tibetan Plateau margin from apatite (U-Th)/He ages, *Earth Planet. Sci. Lett.*, *296*, 78–88.

Conrad, C. P., and C. Lithgow-Bertelloni (2002), How mantle slabs drive plate tectonics, *Science*, *298*, 207–209.

Deng, K. L. (1996), *The Formation and Development of Sichuan Basin* [in Chinese with English abstract], pp. 114–124, Geological House, Beijing.

Deng, Q., J. Wang, Z. J. Wang, Y. S. Qiu, Q. X. Yang, X. S. Jiang, and Q. D. Du (2013), New evidence for the age of the Macaoyuan Group on the northern margin of the Yangtze block, south China—Implications for stratigraphic correlation and palaeogeographic framework [in Chinese with English abstract], *Geol. Bull. China*, *32*(4), 631–638.

Doglioni, C., E. Carminati, M. Cuffaro, and S. Davide (2007), Subduction kinematics and dynamic constraints, *Earth Sci. Rev.*, *83*, 125–175.

Dong, S. W., J. M. Hu, W. Shi, Z. Y. Zhang, and G. Liu (2006), Jurassic superposed folding in the Daba Mountains, central China [in Chinese with English abstract], *Acta Geosci. Sin.*, *27*(5), 403–410.

Dong, S. W., R. Gao, A. Yin, T. L. Guo, Y. Q. Zhang, J. M. Hu, J. H. Li, W. Shi, and Q. S. Li (2013), What drove continued continent-continent convergence after ocean closure? Insights from high-resolution seismic-reflection profiling across the Daba Shan in central China, *Geology*, *41*, 671–674.

Dong, Y. P., G. W. Zhang, S. C. Lai, D. W. Zhou, and B. Q. Zhu (1999), An ophiolitic tectonic melange first discovered in Huashan area, south margin of Qinling orogenic belt, and its tectonic implications, *Sci. China Ser. D*, *42*, 292–301.

Dong, Y. P., G. W. Zhang, X. Zhao, A. P. Yao, and X. M. Liu (2004), Geochemistry of the subduction-related magmatic rocks in the Dahong Mountains, northern Hubei Province: Constraint on the existence and subduction of the eastern Mianlue oceanic basin, *Sci. China Ser. D*, *47*, 366–377.

Dong, Y. P., G. W. Zhang, F. Neubauer, X. M. Liu, J. Genser, and C. Hauzenberger (2011), Tectonic evolution of the Qinling orogen, China: Review and synthesis, *J. Asian Earth Sci.*, *41*, 213–237.

Enkelmann, E., L. Ratschbacher, R. Jonckheere, R. Nestler, M. Fleischer, R. Gloaguen, B. R. Hacker, Y. Q. Zhang, and Y. S. Ma (2006), Cenozoic exhumation and deformation of northeastern Tibet and the Qinling: Is Tibetan lower crustal flow diverging around the Sichuan Basin, *Geol. Soc. Am. Bull.*, *118*(5–6), 651–671.

Enkin, R. J., Z. Yang, Y. Chen, and V. Courtillot (1992), Paleomagnetic constraints on the geodynamic history of the major blocks of China from Permian to the present, *J. Geophys. Res.*, *97*, 13,953–13,989, doi:10.1029/92JB00648.

Forsyth, D., and S. Uyeda (1975), On the relative importance of the driving forces of plate motion, *Geophys. J. R. Astron. Soc.*, *43*, 163–200.

Gao, R., H. Y. Wang, A. Yin, S. W. Dong, Z. Y. Kuang, A. V. Zuza, W. H. Li, and X. S. Xiong (2013), Tectonic development of the northeastern Tibetan Plateau as constrained by high-resolution deep seismic reflection data, *Lithosphere*, *5*, 555–574.

Gilder, S., and V. Courtillot (1997), Timing of the north-south China collision from new middle to late Mesozoic paleomagnetic data from the north China block, *J. Geophys. Res.*, *102*, 17,713–17,727, doi:10.1029/97JB01201.

Gleadow, A. J. W., I. R. Duddy, J. F. Lovering, and B. R. Griffith (1983), Fission track analysis: A new tool for the evaluation of thermal histories and hydrocarbon potential—Developing for the future, *APEA J.*, *23*, 93–102.

Gong, H. J., L. M. Zhu, B. Y. Sun, B. Li, and B. Guo (2009), Zircon U-Pb ages and Hf isotope characteristics and their geological significance of the Shahewan, Caoping and Zhashui granitic plutons in the South Qinling orogen, *Acta Petrol. Sin.*, *25*, 248–264.

Hacker, B. R., and Q. C. Wang (1995), $^{40}Ar/^{39}Ar$ geochronology of ultrahigh-pressure metamorphism in central China, *Tectonics*, *14*, 994–1006, doi:10.1029/95TC00932.

Hacker, B. R., L. Ratschbacher, L. Webb, T. Ireland, D. Walker, and S. W. Dong (1998), U/Pb zircon ages constrain the architecture of the ultrahigh-pressure Qinling-Dabie Orogen, China, *Earth Planet. Sci. Lett.*, *161*, 215–230.

Hacker, B. R., L. Ratschbacher, L. E. Webb, M. McWilliams, T. Ireland, A. Calvert, S. W. Dong, H. R. Wenk, and D. Chateigner (2000), Exhumation of the ultrahigh-pressure continental crust in east central China: Late Triassic-Early Jurassic extension, *J. Geophys. Res.*, *105*, 13,339–13,364, doi:10.1029/2000JB900039.

Hacker, B. R., L. Ratschbacher, and J. G. Liou (2004), Subduction, collision, and exhumation in the untrahigh-pressure Qinling-Dabie orogen, *Geol. Soc. Spec. Publ.*, *226*, 157–175.

Hacker, B. R., W. R. Simon, L. Ratschbacher, G. Marty, and G. George (2006), High-temperature geochronology constraints on the tectonic history and architecture of the ultrahigh-pressure Dabie-Sulu orogen, *Tectonics*, *25*, TC5006, doi:10.1029/2005TC001937.

Hacker, B. R., P. B. Kelemen, and M. D. Behn (2011), Differentiation of the continental crust by relamination, *Earth Planet. Sci. Lett.*, *307*(3), 501–516.

Harrison, T. M., A. Yin, M. Grove, O. M. Lovera, F. J. Ryerson, and X. H. Zhou (2000), The Zedong Window: A record of superposed Tertiary convergence in southeastern Tibet, *J. Geophys. Res.*, *105*, 19,211–19,230, doi:10.1029/2000JB900078.

Hubei Bureau of Geology and Mineral Resources (1990), *Regional Geology of the Hubei Province* [in Chinese with English summary], pp. 1–705, Geological Press, Beijing.

He, J. K., H. F. Lu, Q. L. Zhang, and B. Zhu (1997), The thrust tectonics and it's transpressive geodynamics in southern Dabashan Mountains [in Chinese with English abstract], *Geol. J. China Univ.*, *3*(4), 419–428.

He, J. K., H. F. Lu, and B. Zhu (1999), The tectonic inversion and its geodynamic processes in northern Daba Mountains of eastern Qinling orogenic belt [in Chinese with English abstract], *Sci. Geol. Sin.*, *34*(2), 139–153.

Hu, J. M., J. T. Cui, Q. R. Meng, and C. Y. Zhao (2004), The U–Pb Age of zircons separated from the Zhashui granite in Qinling orogen and its significance, *Geol. Rev.*, *50*, 323–329.

Hu, J. M., W. Shi, H. J. Qu, H. Chen, G. L. Wu, and M. Tian (2009), Mesozoic deformation of Dabashan curvilinear structural belt of Qinling orogen [in Chinese with English abstract], *Earth Sci. Front.*, *16*(3), 49–68.

Hu, J. M., H. Chen, H. J. Qu, G. L. Wu, J. X. Yang, and Z. Y. Zhang (2012), Mesozoic deformations of the Dabashan in the southern Qinling orogen, central China, *J. Asian Earth Sci.*, *47*, 171–184.

Hu, S. B., A. Raza, K. Min, B. P. Kohn, P. W. Reiners, R. A. Ketcham, J. Y. Wang, and A. J. W. Gleadow (2006), Late Mesozoic and Cenozoic thermotectonic evolution along a transect from the north China craton through the Qinling orogen into the Yangtze craton, central China, *Tectonics*, *25*, TC6009, doi:10.1029/2006TC001985.

Hu, Z. Q. (2011), Studies of tectonic evolution and thermochronology in the northern upper Yangtze region, doctoral dissertation [in Chinese with English abstract], pp. 1–154, Hefei Univ. of Technology.

Huang, K. N., and N. D. Opdyke (1991), Paleomagnetism of Jurassic rocks from southwestern Sichuan and the timing of the closure of the Qinling suture, *Tectonophysics*, *200*, 299–316.

Jiang, Y. H., G. D. Jin, S. Y. Liao, Q. Zhou, and P. Zhao (2010), Geochemical and Sr–Nd–Hf isotopic constraints on the origin of Late Triassic granitoids from the Qinling orogen, central China: Implications for a continental arc to continent–continent collision, *Lithos*, *117*, 183–197.

Jiao, W. F., Y. B. Wu, S. H. Yang, M. Peng, and J. Wang (2009), The oldest basement rock in the Yangtze Craton revealed by zircon U-Pb age and Hf isotope composition, *Sci. China Ser. D*, *52*, 1393–1399.

Jin, W. J., Q. Zhang, D. F. He, and X. Q. Jia (2005), SHRIMP dating of adakites in western Qinling and their implications, *Acta Petrol. Sin.*, *21*, 959–966.

Kapp, P., M. A. Murphy, A. Yin, T. M. Harrison, L. Ding, and J. H. Guo (2003), Mesozoic and Cenozoic tectonic evolution of the Shiquanhe area of western Tibet, *Tectonics*, *22*(4), 1029, doi:10.1029/2001TC001332.

Li, J. H., Y. Q. Zhang, W. Shi, H. L. Li, and S. W. Dong (2009), Tectonic deformation features of Shennongjia region in eastern Dabashan foreland structural belt [in Chinese with English abstract], *J. Geomech.*, *15*(2), 162–177.

Li, J. H., Y. Q. Zhang, S. W. Dong, W. Shi, and H. L. Li (2010), Apatite fission track thermochronologic constraint on Late Mesozoic uplifting of the Fenghuangshan basement uplift [in Chinese with English abstract], *Chin. J. Geol.*, *45*(4), 969–986.

Li, J. H., Y. Q. Zhang, X. B. Xu, S. W. Dong, and T. D. Li (2012), Zircon U-Pb LA-ICP-MS dating of Fenghuangshan pluton in northern Daba Mountains and its implications to tectonic setting [in Chinese with English abstract], *Geol. Rev.*, *58*(2), 581–593.

Li, J. H., Y. Q. Zhang, S. W. Dong, and W. Shi (2013), Structural and geochronological constraints on the Mesozoic tectonic evolution of the North Dabashan zone, South Qinling, central China, *J. Asian Earth Sci*, *64*, 99–114.

Li, J. H., Y. Q. Zhang, S. W. Dong, and S. T. Johnston (2014), Cretaceous tectonic evolution of south China: A preliminary synthesis, *Earth Sci. Rev.*, *134*, 98–136.

Li, S. L., W. D. Mooney, and J. C. Fan (2006), Crustal structure of mainland China from deep seismic sounding data, *Tectonophysics*, *420*, 239–252, doi:10.1016/j.tecto.2006.01.026.

Li, S. Z., T. M. Kusky, L. Wang, G. W. Zhang, S. C. Lai, X. C. Liu, S. W. Dong, and G. C. Zhao (2007), Collision leading to multiple-stage large-scale extrusion in the Qinling orogen: Insights from the Mianlue suture, *Gondwana Res.*, *12*, 121–143.

Li, Z. K., and Y. Y. Ding (2007), A tentative discussion on characteristics of the Daba Mountain nappe structure, *Geophys. Geochem. Explor.*, *31*, 495–498.

Lin, J. L., W. Y. Zhang, and M. Fuller (1985), Preliminary Phanerozoic polar wander path for the north and south China blocks, *Nature*, *313*, 444–449.

Liu, S. G., Z. W. Li, and S. Liu (2006), *Formation and Evolution of Dabashan Foreland Basin and Fold-and-Thrust Belt, Sichuan, China* [in Chinese with English abstract], pp. 1–248, Geological House, Beijing.

Liu, X. M., S. Gao, C. R. Diwu, and W. L. Ling (2008), Precambrian crustal growth of Yangtze Craton as revealed by detrital zircon studies, *Am. J. Sci.*, *308*, 421–468.

Lu, S. N., and L. S. Qu (1987), Characteristics of the Sinian glaciogenic rocks of the Shennongjia region, Hubei Province, China, *Precambrian Res.*, *36*, 127–142.

Luo, K. L., and H. S. Duanmu (2001), Timing of Early Paleozoic igneous rocks in the Daba Mountains [in Chinese with English abstract], *Reg. Geol. China*, *20*(3), 262–266.

Marshak, S. (2004), Salients, recesses, arcs, oroclines, and syntaxes—A review of ideas concerning the formation of map-view curves in fold-thrust belts, in *Thrust Tectonics and Hydrocarbon Systems*, AAPG Mem., vol. 82, edited by K. R. McClay, pp. 131–156, Am. Assoc. Petrol. Geol., Tulsa, Okla.

McCaffrey, R., and J. Nabalek (1998), Role of oblique convergence in the active deformation of the Himalayas and southern Tibet plateau, *Geology*, *26*(8), 691–694.

McDougall, I., and T. M. Harrison (1999), *Geochronology and Thermochronology by the $^{40}Ar/^{39}Ar$ Method*, 2nd ed., 288 pp., Oxford Univ. Press, Oxford, U. K.

Mei, L. F., Z. Q. Liu, J. G. Tang, C. B. Shen, and Y. Y. Fan (2010), Mesozoic intra-continental progressive deformation in western Hunan-Hubei-Eastern Sichuan Provinces of China: Evidence from apatite fission track and balanced cross-section [in Chinese with English abstract], *Earth Sci, J. China Univ. Geosci.*, *35*(2), 161–174.

Meng, Q. R., and G. W. Zhang (1999), Timing of collision of the north and south China blocks: Controversy and reconciliation, *Geology*, *27*, 123–126, doi:10.1130/0091-7613(1999)0272.3.CO;2.

Meng, Q. R., and G. W. Zhang (2000), Geologic framework and tectonic evolution of the Qinling orogen, central China, *Tectonophysics*, *323*, 183–196.

Meng, Q. R., E. Wang, and J. M. Hu (2005), Mesozoic sedimentary evolution of the northwest Sichuan Basin: Implication for continued clockwise rotation of the south China block, *Geol. Soc. Am. Bull.*, *117*, 396–410.

Murphy, M. A., A. Yin, T. M. Harrison, S. B. Durr, Z. Chen, F. J. Ryerson, W. S. F. Kidd, X. Wang, and X. Zhou (1997), Did the Indo-Asian collision alone create the Tibetan plateau, *Geology*, *25*, 719–722.

Nie, S., and D. Rowley (1994), Comment of "Paleomagnetic constraints on the geodynamic history of the major blocks of China from the Permian to the present" by Enkins et al, *J. Geophys. Res.*, *99*, 18,035–18,042, doi:10.1029/93JB03283.

Pei, X. Z., Y. Li, S. N. Lu, Z. H. Chen, S. P. Ding, B. Hu, Z. C. Li, and H. B. Liu (2005), Zircon U– Pb ages of the Guanzizhen intermediate-basic igneous complex in Tianshui area, West Qinling, and their geological significance, *Geol. Bull. China*, *24*, 23–29.

Pei, X. Z., S. P. Ding, Z. C. Li, Z. Q. Liu, G. Y. Li, R. B. Li, F. Wang, and F. J. Li (2007), LA-ICPMS zircon U–Pb dating of the Gabbro from the Guanzizhen Ophiolite in the North Margin of the Western Qinling and its geologic significance, *Acta Geol. Sin.*, *81*, 1550–1561.

Qiu, Y. M., S. Gao, N. J. McNaughton, D. I. Groves, and W. L. Ling (2000), First evidence of 3.2 Ga continental crust in the Yangtze craton of south China and its implications for Archean crustal evolution and Phanerozoic tectonics, *Geology*, *28*, 11–14.

Ratschbacher, L., B. R. Hacker, L. E. Webb, M. McWilliams, T. Ireland, S. W. Dong, A. Calvert, D. Chateigner, and H. R. Wenk (2000), Exhumation of the ultrahigh-pressure continental crust in east central China: Cretaceous and Cenozoic unroofing and the Tan-Lu fault, *J. Geophys. Res.*, *105*, 13,303–13,338, doi:10.1029/2000JB900040.

Ratschbacher, L., B. R. Hacker, A. Calvert, L. E. Webb, J. C. Grimmera, M. O. McWilliamse, T. Irelandf, S. W. Dong, and J. M. Hu (2003), Tectonics of the Qinling (central China): Tectonostratigraphy, geochronology and deformation history, *Tectonophysics*, *366*, 1–53.

Ratschbacher, L., L. Franz, E. Enkelmann, R. Jonckheere, A. Pörschke, B. R. Hacker, S. Dong, and Y. Zhang (2006), The Sino-Korean–Yangtze suture, the Huwan detachment, and the Paleozoic–Tertiary exhumation of (ultra) high-pressure rocks along the Tongbai–Xinxian–Dabie Mountains, in *Ultrahigh-Pressure Metamorphism: Deep Continental Subduction*, edited by B. R. Hacker, W. C. McClelland, and J. G. Liu, *Geol. Soc. Am. Spec. Pap.*, 403, 44–75, Boulder, Colo., doi:10.1130/2006.2403(03).

Reiners, P. W., T. L. Spell, S. Nicolescu, and K. A. Zanetti (2004), Zircon (U-Th)/He thermochronometry: He diffusion and comparisons with $^{40}Ar/^{39}Ar$ dating, *Geochim. Cosmochim. Acta*, 68, 1857–1887, doi:10.1016/j.gca.2003.10.021.

Richardson, N. J., A. L. Densmore, D. Seward, A. Foweler, M. Wipf, M. A. Ellis, L. Yong, and Y. Zhang (2008), Extraordinary denudation in the Sichuan Basin: Insights from low temperature thermochronology adjacent to the eastern margin of the Tibetan Plateau, *J. Geophys. Res.*, 113, B04409, doi:10.1029/2006JB004739.

Shanxi Bureau of Geology and Mineral Resources (SBGMR) (1989), *Regional Geology of the Shanxi Province* [in Chinese with English summary], pp. 1–698, Geological Press, Beijing.

Shen, C. B., L. F. Mei, Z. P. Xu, J. G. Tang, and P. Tian (2007), Fission track thermochronology evidence for Mesozoic-Cenozoic uplifting of Daba Mountain, central China [in Chinese with English abstract], *Acta Petrol. Sin.*, 23(11), 2901–2910.

Shi, W., S. W. Dong, J. M. Hu, Z. Y. Zhang, and G. Liu (2007), An analysis of superposed deformation and tectonic stress fields of the northern segment of Daba Mountain foreland [in Chinese with English abstract], *Acta Geol. Sin.*, 81(10), 1314–1327.

Shi, W., et al. (2012), Intra-continental Dabashan orocline, southwestern Qinling, central China, *J. Asian Earth Sci.*, 46, 20–38.

Spear, F. S. (1995), *Metamorphic Phase Equilibria and Pressure-Temperature-Time Paths*, pp. 1–799, Mineral. Soc. Am., Chantilly, Va.

Sun, W. D., S. G. Li, and Y. D. Chen (2000), Zircon U-Pb dating of granitoids from South Qinling, central China and their geological significance, *Geochinica*, 29(3), 209–216.

Suppe, J. (1983), Geometry and kinematics of fault-bending folding, *Am. J. Sci.*, 283, 684–721.

Tang, L. J., T. L. Guo, Y. X. Yu, W. Z. Jin, R. F. Li, and Y. Zhou (2007), Salt-related structures in the foreland fold-thrust belt of the northeastern Sichuan Basin, south China, *Acta Geol. Sin.*, 81(8), 1048–1064.

Taylor, M. H., and A. Yin (2009), Active faulting on the Tibetan Plateau and sounding regions: Relationships to earthquakes, contemporary strain, and late Cenozoic volcanism, *Geosphere*, 5(3), 199–214, doi:10.1130/GES00217.1.

Wang, E., Q. Meng, B. C. Burchfiel, and G. Zhang (2003), Mesozoic large-scale lateral extrusion, rotation, and uplift of the Tongbai-Dabie Shan in east China, *Geology*, 31, 307–310.

Wang, J., C. Bao, Z. Lou, and Z. Guo (1989), Formation and development of the Sichuan Basin, *Chin. Sediment. Basins*, 1, 147–163.

Wang, M. Z., and Y. Zhou (1988), Development of the upper Permian section of the western Daba Mountains [in Chinese with English abstract], *J. Xi'an Coll. Geol.*, 10(2), 1–7.

Webb, A. A. G. (2013), Preliminary balanced palinspastic reconstruction of Cenozoic deformation across the Himachal Himalaya (northwestern India), *Geosphere*, 9(3), 572–587.

Yan, D. P., M. F. Zhou, S. B. Li, and G. Q. Wei (2011), Structural and geochronological constraints on the Mesozoic-Cenozoic tectonic evolution of the Longmen Shan thrust belt, eastern Tibetan Plateau, *Tectonics*, 30, TC6005, doi:10.1029/2011TC002867.

Yang, Z. Y., V. Courtillot, J. Besse, X. H. Ma, L. S. Xing, S. J. Xu, and J. X. Zhang (1992), Jurassic paleomagnetic constrains on the collision of the north and south China blocks, *Geophys. Res. Lett.*, 19, 577–580, doi:10.1029/91GL02416.

Yin, A. (2006), Cenozoic tectonic evolution of the Himalayan orogen as constrained by along-strike variation of structural geometry, exhumation history, and foreland sedimentation, *Earth Sci. Rev.*, 76, 1–131.

Yin, A. (2010), Cenozoic tectonics of Asia: A preliminary synthesis, *Tectonophysics*, 488, 293–325.

Yin, A., and S. Nie (1993), An indentation model for the north and south China collision and the development of the Tan-Lu and Honam fault systems, eastern Asia, *Tectonics*, 12, 801–813, doi:10.1029/93TC00313.

Yin, A., and S. Y. Nie (1996), A phanerozoic reconstruction of China and its neighboring regions, in *The Tectonics of Asia*, edited by A. Yin and T. M. Harrison, pp. 442–485, Cambridge Univ. Press, New York.

Yin, A., and M. H. Taylor (2011), Mechanics of V-shaped conjugate strike-slip faults and the corresponding continuum nature of continental deformation, *Geol. Soc. Am. Bull.*, 123(9/10), 1798–1821.

Yin, A., T. M. Harrison, F. J. Ryerson, W. J. Chen, W. S. F. Kidd, and P. Copeland (1994), Tertiary structural evolution of the Gangdese thrust system in southeastern Tibet, *J. Geophys. Res.*, 99, 18,175–18,201, doi:10.1029/94JB00504.

Yin, A., M. W. McRivette, W. P. Burgess, and X. Chen (2007), Cenozoic tectonic evolution of Qaidam basin and its surrounding regions (Part 2): Wedge tectonics in southern Qaidam basin and the Eastern Kunlun Range, in *Whence the Mountains? Inquiries Into the Evolution of Orogenic Systems: A Volume in Honor of Raymond Price*, *Geol. Soc. Am. Spec. Pap.*, vol. 433, edited by J. W. Sears, T. A. Harms, and C. A. Evenchick, pp. 369–390, Boulder, Colo., doi:10.1130/2007.2433(18).

Yin, A., X. Chen, M. W. McRivette, L. Wang, and W. Jiang (2008a), Cenozoic tectonic evolution of Qaidam basin and its surrounding regions (Part 1): The North Qaidam thrust system, *Geol. Soc. Am. Bull.*, doi:10.1130/B26180.1.

Yin, A., Y. Q. Dang, X. H. Chen, L. C. Wang, W. M. Jiang, S. P. Zhou, and M. W. McRivette (2008b), Cenozoic evolution of Qaidam Basin and its surrounding regions (Part 3): Structural geology, sedimentation, and tectonic reconstruction, *Geol. Soc. Am. Bull.*, 120, 847–876.

Yin, A., C. S. Dubey, T. K. Kelty, A. A. G. Web, T. M. Harrison, C. Y. Chou, and J. Célérier (2010), Geologic correlation of the Himalayan orogen and Indian craton: Part 2. Structural geology, geochronology, tectonic evolution of the Eastern Himalaya, *Geol. Soc. Am. Bull.*, 122(3–4), 360–395.

Yokoyama, M., Y. Y. Liu, and N. Halim (2001), Paleomagnetic study of Upper Jurassic rocks from the Sichuan Basin: Tectonic aspects for the collision between the Yangtze Block and the north China Block, *Earth Planet. Sci. Lett.*, 193, 273–285.

Zhang, G. W., B. R. Zhang, X. C. Yuan, and Q. H. Xiao (2001), *Qinling Orogenic Belt and Continental Dynamics* [in Chinese with English abstract], pp. 1–855, Science Press, Beijing.

Zhang, G. W., S. Y. Cheng, A. L. Guo, Y. P. Dong, S. C. Lai, and A. P. Yao (2004), Mianlue paleo-suture on the southern margin of the Central Orogenic System in Qinling-Dabie—With a discussion of the assembly of the main part of the continent of China [in Chinese with English abstract], *Geol. Bull. China*, 23(9–10), 846–853.

Zhang, Y., Y. P. Dong, T. G. Li, M. S. Yang, S. Y. Cheng, and Y. P. Wang (2009), Magnetic anomaly analysis of the Dabashan fault and its tectonic implications, *Progr. Geophys.*, 24, 1267–1274.

Zhang, Y. Q., W. Shi, J. H. Li, R. R. Wang, H. L. Li, and S. W. Dong (2010), Formation mechanism of the Dabashan foreland arc-shaped structural belt, *Acta Geol. Sin.*, 84(9), 1300–1315.

Zhang, Y. Q., S. W. Dong, J. H. Li, and W. Shi (2011), Mesozoic multi-directional compressional tectonics and formation-reformation of Sichuan Basin [in Chinese with English abstract], *Geol. China*, 38(2), 233–250.

Zhao, X. X., and R. Coe (1987), Palaeomagnetic constraints on the collision and rotation of north and south China, *Nature*, 327, 141–144.

Zou, X. W., Q. F. Duan, Z. Y. Tang, L. Cao, S. Cui, W. Q. Zhao, J. Xia, and L. Wang (2011), SHRIMP zircon U-Pb dating and lithogeochemical characteristics of diabase from Zhenping area in North Daba Mountain [in Chinese with English abstract], *Geol. China*, 38(2), 282–291.